Johanna Ranninger, BSc

Development and Characterization of Pd-based Catalysts for the alkaline Direct Ethanol Fuel Cell

MASTERARBEIT

zur Erlangung des akademischen Grades

Diplom-Ingenieurin

Masterstudium Technische Chemie

eingereicht an der

Technischen Universität Graz

Betreuer

Assoc. Prof. Dipl.-Ing. Dr.techn. Viktor Hacker

Institut für Chemische Verfahrenstechnik und Umwelttechnik

Zweitbetreuer
Dipl.-Ing. Bernd Cermenek, BSc

Graz, Oktober 2017

EIDESSTATTLICHE ERKLÄRUNG

Ich erkläre an Eides statt, dass ich die vorliegende Arbeit selbstständig verfasst, andere als die angegebenen Quellen/Hilfsmittel nicht benutzt, und die den benutzten Quellen wörtlich und inhaltlich entnommenen Stellen als solche kenntlich gemacht habe. Das in TUGRAZonline hochgeladene Textdokument ist mit der vorliegenden Masterarbeit identisch.

Datum

Unterschrift

Danksagung

An dieser Stelle möchte ich mich bei allen bedanken, die mich während der Ausarbeitung und Anfertigung der Masterarbeit unterstützt haben.

Besonderer Dank gebührt Professor Viktor Hacker für die Möglichkeit meine Masterarbeit auf dem Gebiet der Direkt-Ethanol-Brennstoffzelle verfassen zu können und seine Unterstützung während dieser Zeit.

Bei DI Bernd Cermenek möchte ich mich recht herzlich für die engagierte Betreuung meiner Masterarbeit und die tolle Zusammenarbeit bedanken. Vielen Dank für deinen Einsatz, der es mir ermöglicht hat, während der Zeit meiner Masterarbeit sehr viel Neues zu lernen und mich weiterzuentwickeln.

DI Norbert Kienzl möchte ich für die Durchführung und Auswertung der ICP-OES Messungen danken.

Bei DI Ilena Grimmer und Paul Zorn möchte ich mich für ihre Unterstützung bei der Durchführung der Zellmessungen bedanken. Natürlich gilt mein Dank auch der gesamten Brennstoffzellenarbeitsgruppe für das freundliche Arbeitsklima, die Unterstützung und den netten Umgang.

Meinen Eltern, meinen Schwestern Barbara und Christina, sowie meinem Freund Silvan und meinen Freunden möchte ich für die fortwährende moralische Unterstützung und den Rückhalt, nicht nur während der Masterarbeit, sondern während meiner gesamten Studienzeit danken.

Abstract

The alkaline direct ethanol fuel cell (DEFC) generates CO_2-neutral electricity. For applications in commercial products, however, the conversion efficiency is too low due to the sluggish kinetics of the electrochemical anode reaction. The ethanol oxidation reaction (EOR) at the anode is incomplete leading mainly to the final product acetic acid instead of CO_2 and water. During the partial oxidation of ethanol, only four electrons instead of theoretical twelve electrons are released. Therefore, the catalyst development comprises improvements in activity, stability as well as byproduct tolerance.

Novel PdNiBi/C catalysts with different molar compositions on the carbon black carrier Vulcan XC72R were synthesized via the simultaneous reduction method and *ex-situ* characterized in thin-film rotating disk electrode measurements by means of cyclic voltammetry (CV) and chronoamperometry (CA). The atomic ratios of Pd, Ni and Bi were varied to develop catalysts with high activity and stability. The $Pd_{60}Ni_{20}Bi_{20}$/C exhibits the best results in terms of stability and byproduct tolerance. The highest activity is reached by the $Pd_{70}Ni_{20}Bi_{10}$/C catalyst. Both the $Pd_{60}Ni_{20}Bi_{20}$/C and $Pd_{70}Ni_{20}Bi_{10}$/C catalyst were also investigated in a single cell measurement using a liquid electrolyte (6 M KOH) and a perovskite based cathode catalyst and compared to the reference catalyst (Pd/C).

Kurzfassung

Die alkalische Direkt-Ethanol-Brennstoffzelle (DEFC) erzeugt CO_2-neutralen elektrischen Strom. Für die Anwendung in kommerziellen Produkten ist der Umwandlungswirkungsgrad aufgrund der kinetisch gehemmten elektrochemischen Anodenreaktionen zu niedrig. Die Ethanoloxidationsreaktion (EOR) an der Anode läuft unvollständig ab und als Endprodukt entsteht vorwiegend Essigsäure anstatt von CO_2 und Wasser. Bei der partiellen Oxidation von Ethanol entstehen nur vier Elektronen anstelle von theoretisch zwölf Elektronen. Die Katalysatorentwicklung umfasst daher sowohl Verbesserungen der Aktivität, der Stabilität, als auch der Nebenprodukttoleranz.

Es wurden neuartige PdNiBi/C Katalysatoren in verschiedenen atomaren Zusammensetzungen auf dem Kohlenstoffträger Vulcan XC72R mit der simultanen Reduktionsmethode hergestellt und mittels Cyclovoltammetrie (CV) und Chronoamperometrie (CA) an der rotierenden Scheibenelektrode charakterisiert. Die molaren Anteile von Pd, Ni und Bi wurden variiert, um Katalysatoren mit hoher Aktivität und Stabilität zu erhalten. Der $Pd_{60}Ni_{20}Bi_{20}$/C Katalysator zeichnet sich durch die sehr gute Stabilität und Nebenprodukttoleranz aus. Die höchste Aktivität erreicht der $Pd_{70}Ni_{20}Bi_{10}$/C Katalysator. Die beiden Katalysatoren $Pd_{60}Ni_{20}Bi_{20}$/C und $Pd_{70}Ni_{20}Bi_{10}$/C wurden ebenfalls in einer Einzelzelle mit flüssigem Elektrolyten (6 M KOH) und einem Perowskit basierten Kathodenkatalysator getestet und mit dem Referenzkatalysator (Pd/C) verglichen.

Content

1 Introduction

1.1 General

The dramatic effects of air and water pollution are not only visible in big cities, where people have to suffer under smog, but also for example remote coral riffs die off because of the increased water temperature. As the worldwide energy demand is expected to rise even further in the next thirty years, measures to exploit renewable resources are more extensively investigated. In OECD countries, the energy consumption is expected to grow by 0.6% per year whereas in non-OECD countries the increase is estimated to be as high as 1.9% per year. That results in a worldwide energy consumption growth of 1.4% per year [1]. Especially, China and India are expected to contribute the most to the increasing energy demand, not only because of their growing populations but also due to the living standards that will increase. The current dependence on fossil fuels to meet the increasing energy demand and the resulting environmental causes leave no doubt that new ideas have to be developed in order to ensure a clean and stable energy supply network.

The main problem when it comes to the usage of renewable resources for energy production is that the energy cannot be generated on demand. Instead more energy than needed is produced at once and some other time when energy is required it cannot be produced. The best examples are solar panels that generate electricity for the household. In that case, the highest efficiency is reached during noon. However, most people are not at home during that time and the generated electricity is lost if it cannot be stored. In the morning, on the other hand, a lot of electricity is needed that the solar panels cannot provide. To solve that problem, electric energy storage systems, have to be investigated. These energy storage systems can be classified according to their storage form. Electrical energy storage (e.g.: capacitors), mechanical storage (e.g.: flywheels), chemical energy storage (e.g.: batteries, solar hydrogen) and thermal energy storage (e.g.: steam/hot water accumulators) are possible [2]. However, in all those storage systems energy is lost in every conversion step. The goal is to develop technologies in which the losses are minimized.

Another important topic when it comes to climate change is the mobility. Conventional cars which run on diesel or gasoline are one of the main factors leading

to air pollution in the cities. Right now electric cars become more and more popular. Those cars use electricity which is stored in a lithium-ion battery.

Those electric cars are claimed to be renewable because they do not use fossil fuels but, at a closer look, they are not totally renewable. When talking about electric cars, the source of the electricity has to be taken into account. In 2014, Austria used around 90% of the energy sources for electricity production from renewable resources (see Table 1-1) [3].

Table 1-1: Energy sources for electricity production in Austria in 2014 [3].

Known renewable energy source %	Known fossil energy source %	Unknown primary energy source %	Unknown Origin ENTSO-E-Mix %
89.10	10.36	0.26	0.27

The ratio of renewable energy source used in Austria is relatively high compared to other countries like for example the United States of America. In 2014, more than 39% of the produced electricity originated from coal which is well-known as one of the main contributors to air pollution. Further major electricity sources were natural gas with a share of 28% and nuclear power with about 19% [4].

The other alternative to cars which run on gasoline and diesel are fuel cell cars powered with hydrogen. However, hydrogen is mainly obtained from the steam reforming process of fossil fuels or natural gas and therefore cannot be considered a renewable resource. A good way to yield renewable hydrogen would be to use electricity obtained from solar energy to perform water electrolysis [5]. Another big challenge when it comes to hydrogen is that the transportation of hydrogen over longer distances is costly. Furthermore, a distribution network does not exist for hydrogen unlike a distribution system for liquid fuels.

Aside from hydrogen, other fuels can be used to run a fuel cell like hydrocarbons, methanol or ethanol. The direct ethanol or methanol fuel cell (DEFC, DMFC) show lower power densities than hydrogen fuel cells, but they have other advantages and therefore other fields of applications. Apart from mobility, stationary or portable applications like chargers for mobile phones and laptops are of big interest. One

great advantage of those fuels is that they are liquid at room temperature which results in an easier transportation, storage and handling. Especially ethanol is considered a promising fuel due to its low toxicity and high energy density (8.0 kWh kg^{-1}) [6]. Furthermore, it is a carbon-neutral fuel because it is obtained via fermenting sugar containing plants. On the one hand, plants can convert carbon dioxide (CO_2) in presence of water (H_2O) into oxygen (O_2) and glucose. On the other hand, CO_2 is emitted again during the energy utilization process which means a closed carbon cycle. The first generation ethanol is problematic because it uses edible resources, though a lot of research is done to switch to second generation ethanol which is generated from lignocellulose. In the second generation ethanol production, no edible resources have to be used but plant waste can be utilized and competition with food crops can be prevented [7].

1.2 Goal of the master's thesis

Within the course of this master's thesis, anode catalysts for the alkaline direct ethanol fuel cell (DEFC) are developed. The aim is to develop Pt-free catalysts due to high prices and limited abundance of Pt. This work focuses on Pd-based catalysts. The biggest challenge for the alkaline DEFC is to develop an anode catalyst which can cleave the C-C bond in the ethanol molecule. Further goals are to enhance the activity, stability, and byproduct tolerance of Pd based anode catalysts toward ethanol oxidation reaction (EOR). Those parameters for the anode catalyst have to be improved, to make the DEFC competitive for commercial applications.

2 Theory

2.1 Fuel cell basics

Fuel cells (FC) convert the chemical energy of the used fuel directly into electrical energy and heat. The fuels such as hydrogen (H_2), hydrocarbons, ethanol (CH_3CH_2OH), methanol (CH_3OH) and oxygen (O_2) are supplied externally and can be stored in an external tank. There are many different FC types which can be classified according to the used electrolyte as follows:

- Polymer electrolyte membrane fuel cell (PEMFC)
- Alkaline fuel cell (AFC)
- Phosphoric acid fuel cell (PAFC)
- Molten carbonate fuel cell (MCFC)
- Solid oxide fuel cell (SOFC)

There are also other classifications e.g. according to the operating temperature of the fuel cell system. PEMFC and AFC are usually operated at low temperature (up to 100 °C), PAFCs, also called high temperature PEMFCs, operate at medium temperatures (100 °C - 250 °C), MCFC (around 600 °C) and SOFC (800 °C – 1000 °C) are classified as high temperature fuel cells [8].

PEMFC has the broadest range of application including mobility, whereas MCFC and SOFC are mainly used in industrial stationary applications. Alkaline fuel cells have usually smaller dimensions and can be used for stationary and mobile applications.

2.2 Direct alcohol fuel cell (DAFC)

The use of alcohols as fuels has some important advantages compared to the hydrogen fueled PEMFCs. Alcohols like methanol, ethanol, ethylene glycol or glycerol are liquid at room temperature which ensures an easier storage and transportation of the fuel. The infrastructure to distribute liquid fuels for mobility already exists, however, this is not the case concerning the infrastructure of hydrogen

fuel stations. Furthermore, alcohols exhibit high energy densities. The direct methanol fuel cell (DMFC) is the best investigated direct alcohol fuel cell system with a gravimetric energy density of 6000 Wh kg^{-1} for methanol [9]. However, the sluggish kinetics for the oxidation of any alcohol leads to worse power output compared to the PEMFCs. Therefore, further research is required to enhance the activity of the anode catalysts in DAFCs [10].

Most DMFCs operate in acidic medium using a proton exchange membrane mainly Nafion and Pt-based catalysts. Even though there are many different commercially available DMFC systems compared to other DAFCs, some disadvantages have to be considered [9]. First, the Pt-based catalysts suffer from carbon monoxide (CO) poisoning of reaction intermediates. Furthermore, methanol cross-over through the Nafion membrane can lead to mixed potentials at the cathode and decrease the cell potential. Membrane degradation and carbon corrosion are also observed in acidic DMFCs. Methanol as a fuel is toxic and has a relatively low boiling point (65 °C) compared to other alcohols like ethanol (78 °C) or ethylene glycol (197 °C). A higher boiling point is favorable, because the operation conditions at elevated temperature improves the kinetics at the electrodes. When a fuel with lower boiling point is used, the temperature can only be raised below the boiling point without pressurizing the fuel to keep it in liquid aggregate state. All these disadvantages lead to further research activities in other DAFC systems, especially in the direct ethanol fuel cell (DEFC) [10].

2.3 Direct ethanol fuel cell (DEFC)

Two types of DEFCs can be distinguished according to the electrolyte. In the acidic DEFC, a proton exchange membrane mostly Nafion is used, whereas in the alkaline DEFC, an anion exchange or basic liquid electrolyte can be applied see Figure 2-1.

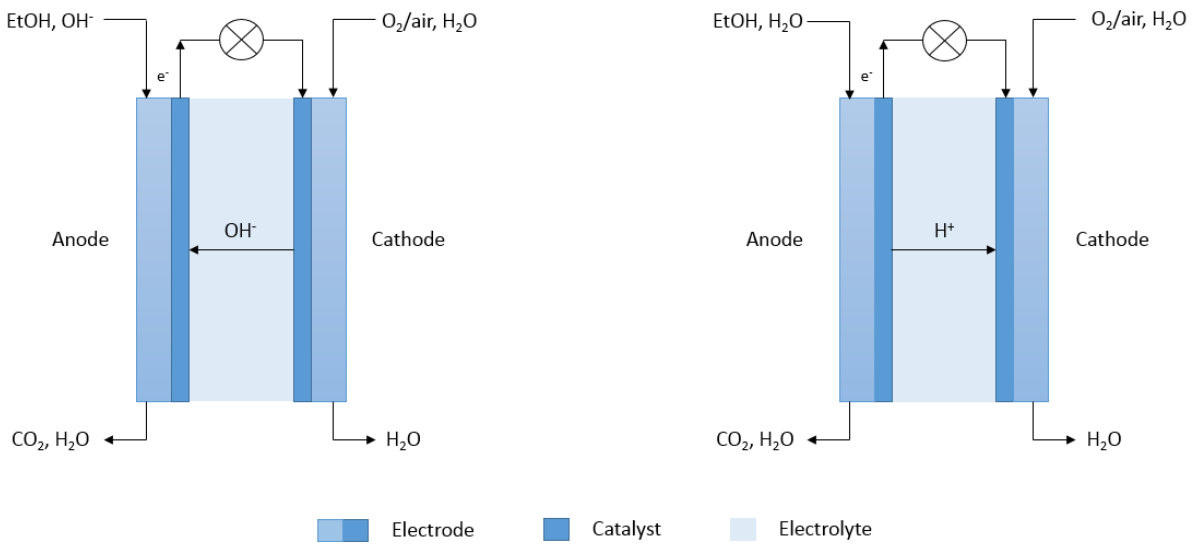

Figure 2-1: Schematic set-up of an alkaline DEFC (left) and an acidic DEFC (right).

In the acidic DEFC, ethanol is oxidized at the anode where protons and CO_2 are generated according to reaction (1). The protons (H^+) are transported through the membrane and CO_2 is emitted. 12 electrons (e^-) which are also generated during the oxidation process are transported through an external circuit and can power a load. At the cathode oxygen is reduced and reacts with the available H^+ ions and e^- to form water (2). The overall reaction processes can be described as the oxidation of ethanol with oxygen to H_2O and CO_2 according to reaction (3).

Anode reaction: $CH_3CH_2OH + 3\ H_2O \rightarrow 12\ H^+ + 2\ CO_2 + 12\ e^-$ (1)

Cathode reaction: $3\ O_2 + 12\ H^+ + 12\ e^- \rightarrow 6\ H_2O$ (2)

Cell reaction: $CH_3CH_2OH + 3\ O_2 \rightarrow 3\ H_2O + 2\ CO_2$ (3)

In the alkaline DEFC, hydroxide (OH^-) ions are utilized to oxidize ethanol at the anode (4). During that process again 12 e^- are generated which are transported through an external circuit to the cathode. Meanwhile, on the cathode oxygen reacts with electrons and water to OH^- ions which are transported through the membrane and used at the anode for the oxidation of ethanol (5). Additional alkaline solution is provided at the anode to facilitate the oxidation of ethanol. Despite the different processes occurring at the electrodes the overall cell reaction is the same as in the acidic DEFC (see (3) and (6)).

Anode reaction: $CH_3CH_2OH + 12\ OH^- \rightarrow 2\ CO_2 + 9\ H_2O + 12\ e^-$ (4)

Cathode reaction: $3\ O_2 + 6\ H_2O + 12\ e^- \rightarrow 12\ OH^-$ (5)

Cell reaction: $CH_3CH_2OH + 3\ O_2 \rightarrow 3\ H_2O + 2\ CO_2$ (6)

As shown above, the overall cell reactions (3) and (6) are the same for both cells but there are some fundamental differences according to the working principle. For example in the alkaline DEFC, the direction of the ion mobility through the membrane is reversed compared to the acidic DEFC which leads to an inversion of the electro-osmotic pressure and reduces the ethanol cross-over [11].

The alkaline fuel cell is one of the oldest fuel cell systems and was first introduced by Francis Thomas Bacon who started developing alkaline fuel cells in 1933. He used porous Ni as electrodes, a KOH solution as electrolyte and H_2 and O_2 as anode and cathode fuels, respectively [12]. The cell degraded fast due to corrosion of the electrodes, however, F. T. Bacon succeeded to improve the stability of the electrodes after intensive research. His work climaxed in 1959, when he developed the first fully-functional fuel cell, leading to the introduction of the fuel cell technology in the NASA for the Gemini and Apollo space program [12,13].

The biggest problem in such a classical alkaline fuel cell is the carbonation of the electrolyte. The OH^- ions react with CO_2 in the air and the CO_2 formed during the ethanol oxidation to carbonate (CO_3^{2-}) ions (7).

$$2\ OH^- + CO_2 \rightarrow CO_3^{2-} + H_2O \quad (7)$$

This leads to solid precipitation which blocks the pores of the electrodes and leads to an increased pH. Hence, the activity of the oxidation and reduction reactions are reduced as well as the conductivity of the electrolyte [11].

With the development of Polymer Electrolyte Membranes like Nafion, the development of DAFCs was mainly focused on acidic DAFCs, however, in previous years, the development of anion exchange membranes (AEM) lead to new research interests in alkaline DAFCs. When an AEM is applied instead of liquid alkaline electrolyte, the formation of carbonate can be drastically decreased [9,11].

The alkaline DEFC has additional advantages compared to the DEFC using an acidic electrolyte. DAFCs show better polarization characteristics in alkaline media then in acidic media due to improved kinetics on both electrodes. In alkaline media, noble as well as non-noble metals are stable. In particular metals aside from the platinum group can be applied as cathode catalysts like Ni, Ag or perovskite catalysts. As mentioned above the ethanol cross-over is reduced because of the reversed direction of the ion conduction. Furthermore, less catalyst degradation, carbon corrosion and poisoning of the catalyst are observed [10].

Generally, the alkaline DEFC consists of anode, cathode and electrolyte. There are different requirements for each compartment to reach a good cell performance. As mentioned above in an alkaline fuel cell, the electrolyte can be either liquid or a thin membrane.

Liquid electrolytes usually show higher ionic conductivity than AEMs but are affected by carbonation when CO_2 is dissolved in the electrolyte.

Since the development of AEMs, the alkaline FC is becoming more attractive again. Many different AEMs have been developed, whereupon all of them have a polymeric backbone with cationic side chains (see Figure 2-2). The most promising and widely used ones are AEMs produced by the Tokuyama Corporation Japan. The use of OH^- doped polybenzimidazole (PBI) membranes which are known for the use in high temperature PEMFCs and OH^- doped Nafion have also been reported. However, single cells using OH^- doped PBI or Nafion membranes exhibited lower power densities than single cells using AEMs by Tokuyama [16].

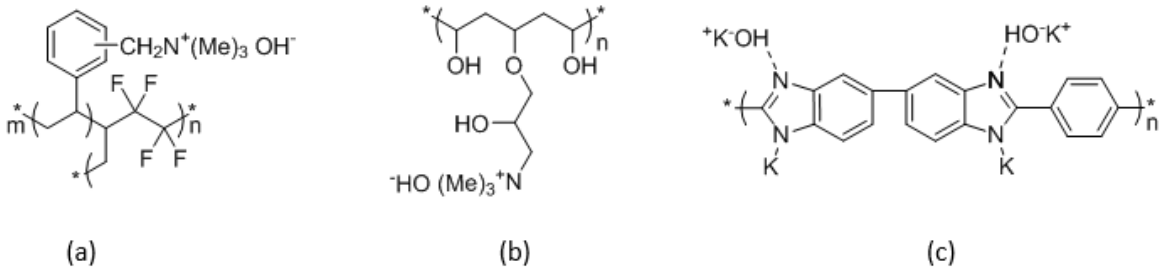

Figure 2-2: Different membrane structures which can be used in alkaline DEFC. (a) functionalized poly(ethylene-co-tetrafluoroethylene) (b) functionalized poly(vinyl alcohol (c) OH^- doped poly(benzimidazole) [13,14,15].

Aside from high ionic conductivity, other factors have to be taken into account when AEMs are developed. The permeability of the educts such as ethanol and O_2 through the membrane should be prevented. Furthermore, the swelling of the membrane has to be limited. The chemical and mechanical stability is crucial for the long-term performance of a membrane because small cracks or pinholes cause fuel cross-over or even short circuit.

At the cathode, oxygen is reduced to OH^- in presence of water. For better distribution of O_2 on the cathode, a gas diffusion layer (GDL), a layer consisting of highly porous conductive material, is often applied beneath the actual catalyst layer. The requirements for the cathode are a good stability in alkaline medium, high activity toward the oxygen reduction reaction (ORR) and inactivity toward the ethanol oxidation reaction (EOR) because ethanol cross-over cannot be totally prevented. Platinum (Pt) is the catalyst of choice in fuel cells operating with an acidic electrolyte. However, Pt is not ethanol tolerant, meaning Pt is also an active catalyst for the EOR. If ethanol passes through the membrane, Pt also catalyzes the EOR leading to mixed potentials at the cathode which decrease the cell voltage. Due to the stability of non-noble metals in alkaline medium, Pt free catalysts are intensively investigated. Tang *et al.* reported Ag/C, Mn_yO_x and Ag/Mn_yO_x/C as materials for cathode catalysts in alkaline DMFC with an activity toward the ORR similar to Pt/C. Aside from the cost reduction, Ag/Mn_yO_x also exhibited higher ethanol tolerance and was more stable in the presence of low concentrations of methanol (0.1 M) than Pt/C [20]. Grimmer *et al.* reported two perovskite cathode catalysts, $La_{0.7}Sr_{0.3}(Fe_{0.2}Co_{0.8})O_3$ and $La_{0.7}Sr_{0.3}MnO_3$, as alternatives to the widely used non-precious Mn_yO_x catalysts. $La_{0.7}Sr_{0.3}MnO_3$ outperformed the Mn_yO_x catalyst in terms of activity and stands out due to the excellent ethanol tolerance [21].

The requirements for catalysts at the anode in the DEFC are high activity toward the ethanol oxidation reaction (EOR), a high tolerance for byproducts formed during the reaction or a low tendency of the catalyst to absorb poisonous species and a high long-term stability. The EOR in acidic media is mostly catalyzed by Pt-based catalysts. However, in alkaline medium, Pd has been reported to outperform Pt as catalyst for the EOR. Xu *et al.* found that the onset potential for the EOR on Pd is shifted to lower potentials compared to the oxidation on Pt. Furthermore, the peak

current obtained from the Pd catalyzed reaction exceeded the peak current of the Pt catalyzed reaction [22]. Additionally, Pd is not only cheaper than Pt but also more abundant in nature [23].

In the complete oxidation of one ethanol molecule, 12 e^- are generated (see (4)). This reaction involves the cleavage of the C-C bond in the ethanol molecule which requires a high energy input and is rarely observed at low temperatures. Liang *et al.* reported a mechanistic study of the EOR process on Pd. The authors found that less than 5% of the ethanol is oxidized to CO_2 and that the main product of the oxidation is acetic acid (see Figure 2-3). During the oxidation of ethanol to acetic acid, only 4 e^- are released instead of 12 e^-. It was also stated that acetaldehyde is an active intermediate which is further oxidized to acetic acid [24].

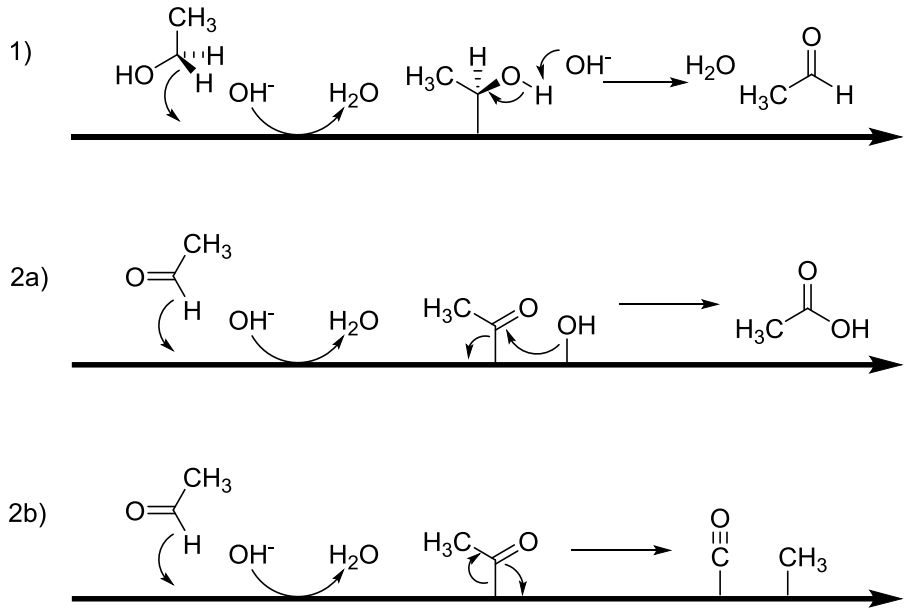

Figure 2-3: Suggested mechanism of the EOR on the catalyst surface in alkaline medium. 1) 1st step: oxidation of ethanol to acetaldehyde. 2a) 2nd step: Further oxidation of acetaldehyde to acetic acid 2b) Theoretical 2nd step: reduction of acetaldehyde via the C-C bond cleavage pathway [10].

In alkaline medium, the kinetics of the ethanol oxidation on various non-Pt based catalysts are enhanced. Pd for example exhibits good activity toward the EOR in alkaline medium [22]. However, the performance of the currently used anode catalysts for the alkaline DEFC is not efficient enough to find broad applications on the market. Therefore, a lot of research is dedicated to anode materials to enhance the EOR performance and to reduce the costs. The most promising techniques are to

find synthesis methods for catalyst nanostructures to enlarge the surface of the active material and to alloy Pd with other metals. The advantage of bi- and trimetallic catalysts is that the additives are mainly cheaper and act as cocatalysts which facilitate the catalytic activity.

Ni is a very promising candidate as cocatalyst for Pd. Shen *et al.* first reported an anode catalyst composed of Pd-NiO/C (C = Vulcan XC-72R). This catalyst has lower onset potential and higher current densities than the Pd-oxide/C catalyst without NiO addition. Furthermore, the Pd-NiO/C catalyst exhibits higher tolerance for poisonous species than Pt-based electrocatalysts [25]. Shen *et al.* described PdNi/C (C = Vulcan XC-72R) catalysts with different atomic ratios. It was reported that the addition of Ni to Pd catalysts increases the activity as well as the stability of the catalyst. The increase in activity was suggested to be due to the affinity of Ni to form Ni-OH_{ads} species which facilitate the oxidation process to acetic acid via the bifunctional mechanism (see Figure 2-3) and also the oxidative removal of poisonous species. Additionally, it was found that if the Ni content was too high, the activity was reduced due to the low conductivity of the Ni oxide species [26].

Aside from Ni, Neto *et al.* reported a positive impact on the performance of the anode catalyst upon adding Bi to Pd. An investigation on PdBi/C (C = Vulcan XC-72R) catalysts with different atomic ratios was performed. PdBi/C catalyst with ratios of (95:05), (90:10), (80:20) and (70:30) were synthesized. Their performances were tested in an electrochemical *ex-situ* measurement and compared to a Pd/C catalyst. For PdBi/C (95:05) and (90:10) it was found that the onset potential was lower compared to Pd/C and that PdBi/C (95:05) exhibited the highest peak current density. In a chronoamperometry measurement the PdBi/C catalysts (95:05 and 90:10) also had the highest currents after 30 minutes. It was stated that the addition of small amounts of Bi facilitates the oxidative removal of adsorbed ethoxy species on the Pd surface. As this is claimed to be the rate-determining step, it can be concluded that the addition of Bi enhances the kinetics and also reduces the poisoning of the catalytic sites [27].

The addition of other elements like phosphorus (P) and zinc (Zn) was also investigated, whereupon, the addition of P to PdNi/C catalyst was reported to give smaller catalyst particle size. The PdNiP and PdNiZn/C (C = Vulcan XC-72R)

catalysts exceeded PdNi/C in terms of peak current and also exhibited a lower onset potential than the PdNi/C catalyst [23,24].

2.3.1 Thermodynamic consideration of reactions in the alkaline DEFC

The EOR that takes place at the anode has a standard potential of E° = -0.74 V [6]. (standard conditions p = 1.0 atm and T = 298.15 K)

$$CH_3CH_2OH + 12\ OH^- \rightarrow 2\ CO_2 + 9\ H_2O + 12\ e^- \qquad E°_{anode} = -0.74\ V$$

The ORR in alkaline medium has a standard potential of E° = 0.40 V [6].

$$O_2 + 2\ H_2O + 4\ e^- \rightarrow 4\ OH^- \qquad E°_{cathode} = 0.40\ V$$

Using the standard potential of the cathode and of the anode, the theoretical or reversible standard cell potential can be calculated via Eq. 2-1:

$$E°_{rev} = E°_{cathode} - E°_{anode} \qquad \text{Eq. 2-1}$$

$$E°_{rev} = 1.14\ V$$

The theoretical cell potential of the DEFC (1.14 V) is similar to that of a PEMFC (1.23 V). Using the Nernst equation (Eq. 2-2), the standard free Gibbs energy, the theoretically available energy provided by the fuel cell system, can be obtained from the theoretical cell potential [30].

$$\Delta G° = -n \cdot F \cdot \Delta E° \qquad \text{Eq. 2-2}$$

$$\Delta G° = -1326\ kJ\ mol^{-1}$$

Where ΔG° is the standard free Gibbs energy, n is the number of electrons transferred in the redox process (12 e^- are transferred in the complete oxidation of one ethanol molecule), F is the Faraday constant (96485 C mol^{-1}) and ΔE° is the standard cell potential (1.14 V) [30].

For the evaluation of a fuel cell system, the efficiency is of interest. The thermodynamic efficiency η_t is the maximal efficiency that can be reached and is calculated from the Gibbs free energy and the enthalpy change ΔH° during the reaction (Eq. 2-4). ΔH° is calculated from enthalpies of formation of the products and the enthalpy of formation of ethanol (Eq. 2-3) [31].

$$\Delta H° = 3 \cdot \Delta H_f [H_2O(l)] + 2 \cdot \Delta H_f [CO_2(g)] - \Delta H_f [C_2H_5OH(l)] \qquad \text{Eq. 2-3}$$

For the alkaline DEFC, ΔG° is -1326 kJ mol^{-1} and ΔH° is -1367 kJ mol^{-1} [31].

$$\eta_t = \frac{\Delta G°}{\Delta H°} \qquad \text{Eq. 2-4}$$

$$\eta_t = 0.97$$

The theoretical efficiency of the DEFC is with 97% very high. However, to calculate the actual efficiency of the DEFC, the thermodynamic efficiency has to be multiplied with the voltage efficiency and the faradaic efficiency.

The voltage efficiency η_E takes the losses in a cell into account. Losses that have to be considered are overpotentials at the anode and cathode, respectively. Overpotentials occur due to sluggish kinetics at the electrodes which reduce the cell voltage. The ohmic drop including the resistances in the electrolyte as well as at the interfaces and the mass transfer limitations also have to be considered (Eq. 2-5) [30].

$$E_{cell} = E_{rev} - (|\eta_a| + |\eta_c| + R_{cell} \cdot |j|) \qquad \text{Eq. 2-5}$$

$$\eta_E = \frac{E_{cell}}{E_{rev}} \qquad \text{Eq. 2-6}$$

$$\eta_E = 0.44$$

E_{rev} is the reversible cell potential of 1.14 V, η_a and η_c are the overpotentials at the anode and cathode and the term $R \cdot |j|$ represents the ohmic drop. For calculations of the voltage efficiency for single cells, the operation voltage is used for E_{cell} (Eq. 2-6). DEFCs are usually operated at 0.5 V leading to a η_E of 0.44 [6].

Finally, the faradaic efficiency η_F (Eq. 2-7) takes the incomplete oxidation of the reactants into account.

$$\eta_F = \frac{n_a}{n_t} \qquad \text{Eq. 2-7}$$

$$\eta_F = 0.33$$

Where n_a is the number of actually transferred electrons and n_t is the number of theoretically transferred electrons. The mainly occurring reaction in the DEFC is the oxidation of ethanol to acetic acid during which only 4 e^- are transferred whereas the total oxidation would give 12 e^-. This leads to a faradaic efficiency η_F of 33%, considering only the oxidation of ethanol to acetic acid. For state-of-the-art alkaline DEFC faradaic efficiencies of 37–54% are obtained because only about 5% of ethanol are oxidized to CO_2 the rest is oxidized to acetic acid [6].

The actual efficiency is calculated by multiplying the thermodynamic, voltage and faradaic efficiency (Eq. 2-8).

$$\eta_{FC} = \eta_t \cdot \eta_E \cdot \eta_F \qquad \text{Eq. 2-8}$$

$$\eta_{FC} = 0.14$$

Comparing the actual efficiency η_{FC} of an alkaline DEFC of around 15–20% to the efficiency assuming a total oxidation of ethanol to CO_2 and H_2O of 48%, the importance on further anode catalyst research is obvious. In a PEMFC, the η_t is 85%, the η_E is 65% and a full oxidation of hydrogen is achieved leading to a total efficiency

η_{FC} of 54%, even though the theoretical efficiency is lower than in the DEFC. In case of a complete oxidation of ethanol, the alkaline DEFC would be a good alternative to the widely used PEMFCs and also to the combustion of gasoline and diesel as energy sources [30].

2.4 Analytics

Generally, a new catalyst for fuel cells has to be tested in an *ex-situ* and an *in-situ* measurement. In the *ex-situ* measurement, the activity of several catalysts can be tested in a fast manner using a rotating disk electrode (RDE). If good results are obtained from the RDE experiment an *in-situ* measurement is performed. Therefore, electrodes are fabricated and further processed to a membrane electrode assembly (MEA). Compared to the RDE experiment, an *in-situ* measurement is a rather time and resource intensive method. However, *ex-situ* measurements have the drawback that the results are not always confirmed in the *in-situ* measurement.

2.4.1 Rotating disk electrode (RDE) measurements

In fuel cell research, rotating disk electrode (RDE) measurements are a very powerful method for catalyst screening. Information about the activity and the stability of catalysts is obtained almost immediately that means more catalysts can be investigated than with solely single cell measurements. A typical RDE set-up is shown in Figure 2-4.

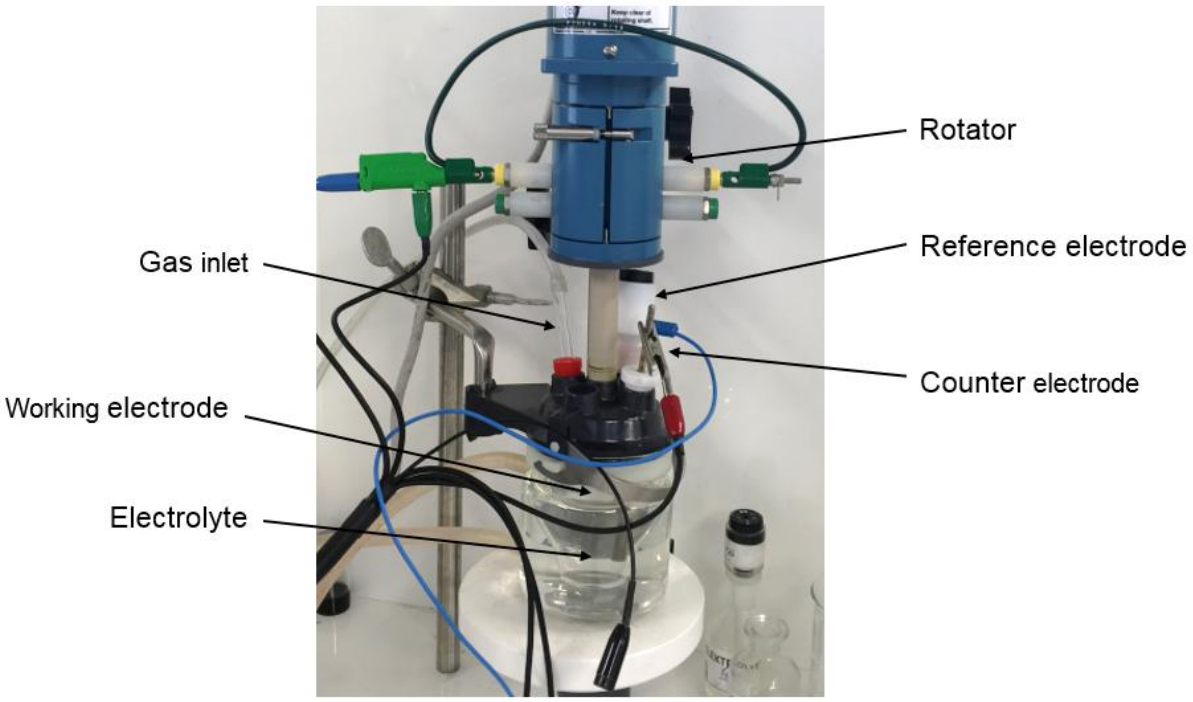

Figure 2-4: Built-up of an RDE measurement.

For the RDE measurement, a three electrode assembly is used. The catalyst material is suspended in solvent and a certain amount is applied on a glassy carbon (GC) electrode which is then dried usually by rotating the electrode to result in a thin catalyst film on the GC electrode. The GC electrode with the catalyst film is used as working electrode. Furthermore, a counter electrode and a reference electrode are used. The electrolyte can be tempered and the gas inlet allows the saturation of the electrolyte with gases like O_2, H_2 or, if inert conditions are required, N_2. Several experiments can be performed using the RDE like cyclic voltammetry, potentio- or amperostatic studies.

2.4.2 Cyclic voltammetry (CV)

Cyclic voltammetry (CV) is a potentiodynamic analysis method that measures the current while the potential is varied with time. In a cyclic voltammogram (CV), reactions at certain potentials can be observed. Figure 2-5 shows a CV of Pd in alkaline medium including typical observable reactions on the Pd surface.

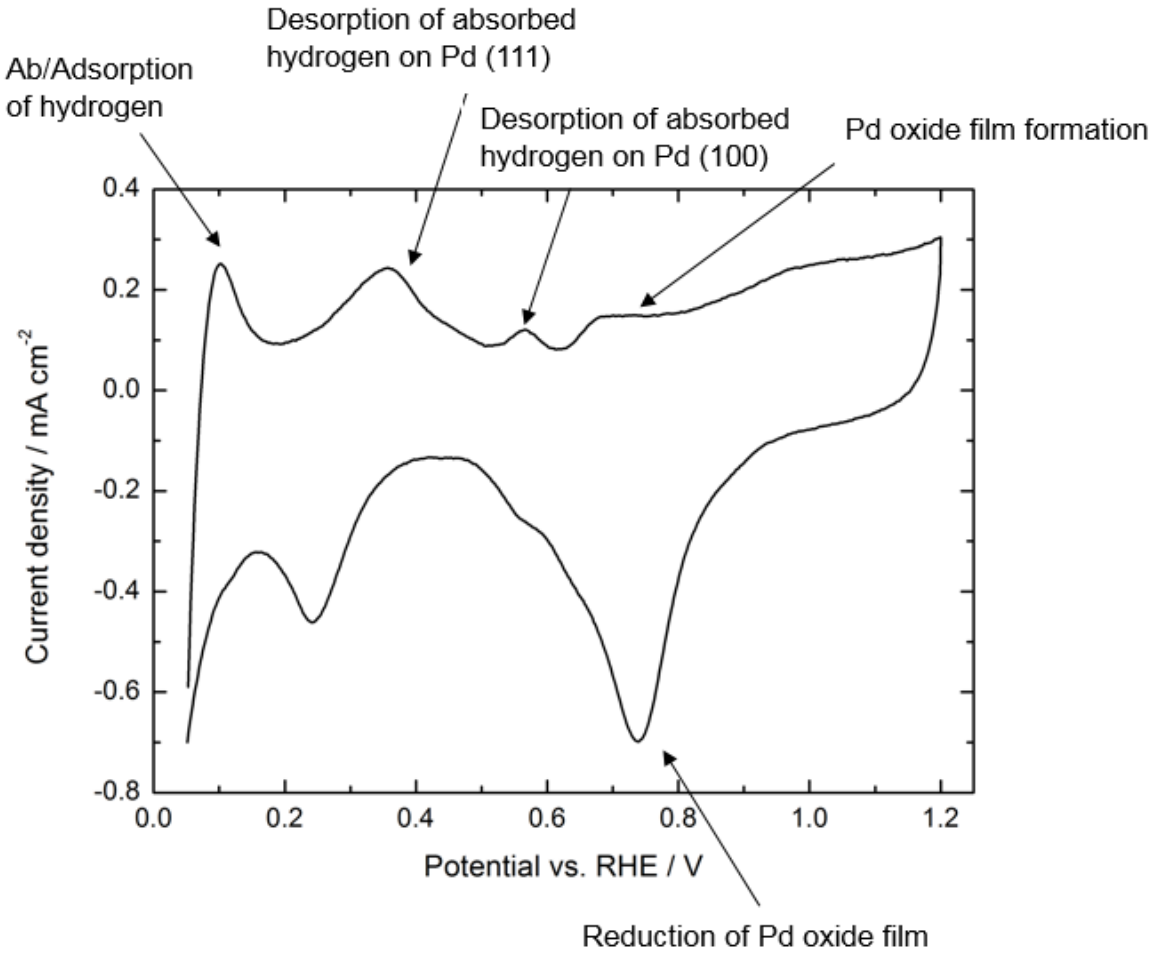

Figure 2-5: CV of a Pd/C catalyst in alkaline medium (1.0 M KOH) at 30 °C and observable reactions on the Pd surface [19,28].

As Pd is a well-known material for hydrogen storage, hydrogen absorption and desorption processes can also be observed in the CV. The first peak around 0.1 V is associated with the absorption and adsorption processes of hydrogen on Pd. Further peaks that can be observed in the CV, in the region between 0.4 V and 0.45 V, are associated with the desorption of absorbed hydrogen on Pd (111) whereas the peak around 0.6 V suggests the desorption of absorbed hydrogen on Pd (100). Other reactions which can be observed are the formation of Pd oxide species on Pd (111), but also on Pd (110) between 0.6 V and 0.8 V. In the backward scan, the peaks around 0.7 and 0.5 V indicate the reduction of PdO species to Pd [32].

The cathodic peak at 0.7 V is often used to estimate the electrochemically active surface area (EASA). For the estimation of the EASA in Pt based catalysts, the area for hydrogen adsorption between 0.05 V and 0.25 V vs. NHE is used [33]. However, as hydrogen does not adsorb onto the Pd surface but diffuses into the crystal lattice,

the area of the reduction peak from PdO to Pd is used to determine the surface because PdO only forms a monolayer at the surface. The estimation of the EASA is achieved by integrating the cathodic peak at 0.7 V (Eq. 2-9) and relating the obtained charge to the Pd content (Eq. 2-10) [20,26].

$$Q_{Pd} = \int I \, dt \qquad \text{Eq. 2-9}$$

$$EASA = \frac{Q_{Pd}}{Q°_{Pd} \cdot A_{electrode} \cdot c_{Pd}} \qquad \text{Eq. 2-10}$$

Where Q_{Pd} is the charge obtained from the integration of the peak approximately at 0.7 V, $Q°_{Pd}$ is the charge necessary to reduce one cm² of PdO to Pd. $A_{electrode}$ is the geometrical area of the electrode and c_{Pd} is the loading of Pd on the electrode. The charge for $Q°_{Pd}$ is 405 µC cm² [34].

Aside from the analysis of the reactions on Pd in an electrolyte, the activity of the catalyst toward the EOR can also be measured. A typical EOR curve of a Pd catalyst in alkaline medium is shown in Figure 2-6.

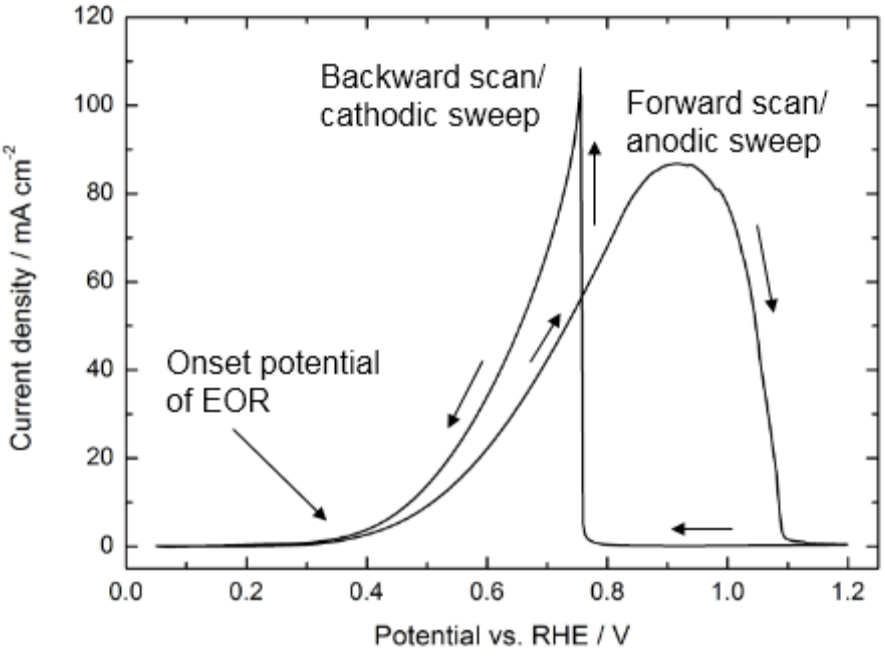

Figure 2-6: Typical EOR curve of a Pd/C catalyst in an aqueous solution (1 M KOH and 1 M EtOH).

In the CV of the EOR, the hydrogen sorption processes are strongly reduced. The oxidation of ethanol starts between 0.3 V and 0.4 V vs. RHE (onset potential) which is observed as an increasing current. The current rises until it reaches its maximum around 0.9 V. Afterwards, a decreasing current is observed due to the formation of PdO which blocks the active sites of Pd. At the upper vertex point (1.2 V vs. RHE), the current is at the baseline level showing that EOR does not occur on PdO. The active sites of Pd can be recovered again when reversing the potential in the cathodic sweep [24]. Qin *et al.* reported that the peak that occurs in the backward scan results from the oxidative removal of reaction intermediates, mainly carbon-based species like -CO or $–CH_3$ [35].

An important parameter to describe the activity of a catalyst toward the EOR is the onset potential. In Figure 2-6 the current starts to increase between 0.3 and 0.4 V which is typical for EOR in alkaline media on Pd based catalysts. Furthermore, the peak current density is a vital parameter. A high peak current density together with a low onset potential in the *ex-situ* measurement indicate a high activity of the catalyst in a single cell measurement. Another crucial characteristic is the byproduct tolerance of the catalyst which indicates the resistance of the catalyst toward poisonous species. As the backward scan is assigned to the oxidative removal of poisonous species, the relation of the peak in the forward scan and the peak in the backward scan gives an outlook how prone the catalyst is to poisoning. Therefore, Lee *et al.* proposed that the byproduct tolerance is calculated from the peak current densities of the forward scan divided by the peak current densities of the backward scan (Eq. 2-11) [36]. Later Sekol *et al.* suggested that it is more accurate to use the total charge of the peaks instead of the peak currents. So the peaks are integrated and the areas of the peaks are divided (Eq. 2-11) [37].

$$\text{byproduct tolerance} = \frac{\mathrm{i}_{\text{forward scan}}}{\mathrm{i}_{\text{backward scan}}} \text{ or } \frac{\mathrm{A}_{\text{forward scan}}}{\mathrm{A}_{\text{backward scan}}} \qquad \text{Eq. 2-11}$$

A high number for the byproduct tolerance means a good resistance toward poisonous species [37].

2.4.3 Chronoamperometry (CA)

Chronoamperometry (CA) is a potentiostatic measurement where the current at a certain potential is measured over a certain period of time. The CA can also be measured in an *ex-situ* measurement via an RDE experiment. The result is an indication for the long-term stability of the catalyst in the fuel cell. When a certain potential is applied, the current decreases. The less the current decreases during a measurement the better is the stability in the actual single cell. An important aspect for the choice of the applied potential for the CA is the peak current density in the previous EOR measurement. The potential should be chosen between the onset potential and the peak potential. Furthermore, it is worth mentioning that each catalyst has a certain potential at which it exhibits the best CA performance which makes the comparison between different catalysts difficult.

2.4.4 Single cell measurements

The *ex-situ* measurement is a good method to test the activity of various catalysts in a fast manner but those results are not always conclusive with the performance of the catalyst in the fuel cell. For exact results, a single cell test has to be performed. For these measurements, anodes and cathodes have to be prepared. The active catalyst material is applied on an electron-conductive carrier which is mainly a carbon based material. Many different electrode fabrication methods can be applied like rolling, drop coating, spray coating or others. Furthermore, if a membrane is chosen as electrolyte, the membrane has to be pretreated, e.g. soaking in acid or base. After the single components (electrodes and membrane) are ready to use, a membrane electrode assembly (MEA) is made by sandwiching the membrane between anode and cathode. Usually, the MEA is hot pressed for better contact between the membrane and the electrodes to reduce the internal resistance. Finally, the MEA is introduced in a single cell and measured in a three electrode assembly using a working, counter and reference electrode.

Potentiostatic or galvanostatic measurements can be performed. Also long-term stability tests like CA can be carried out. The most common measurement is the step

chronopotentiometry. In this measurement, different currents are applied and the resulting potential is measured for one or two minutes. The last measured value or an average of the last measurement points is taken and creates a characteristic U-I curve. When every measured potential is multiplied with the corresponding current density, an additional power density curve can be obtained.

2.4.5 Polarization curve characteristics

A typical polarization curve is shown in Figure 2-7. In the single cell measurement, the reversible cell voltage is not reached. Several processes take place which reduce the cell potential. Some of them have already been mentioned in chapter 2.3.1.

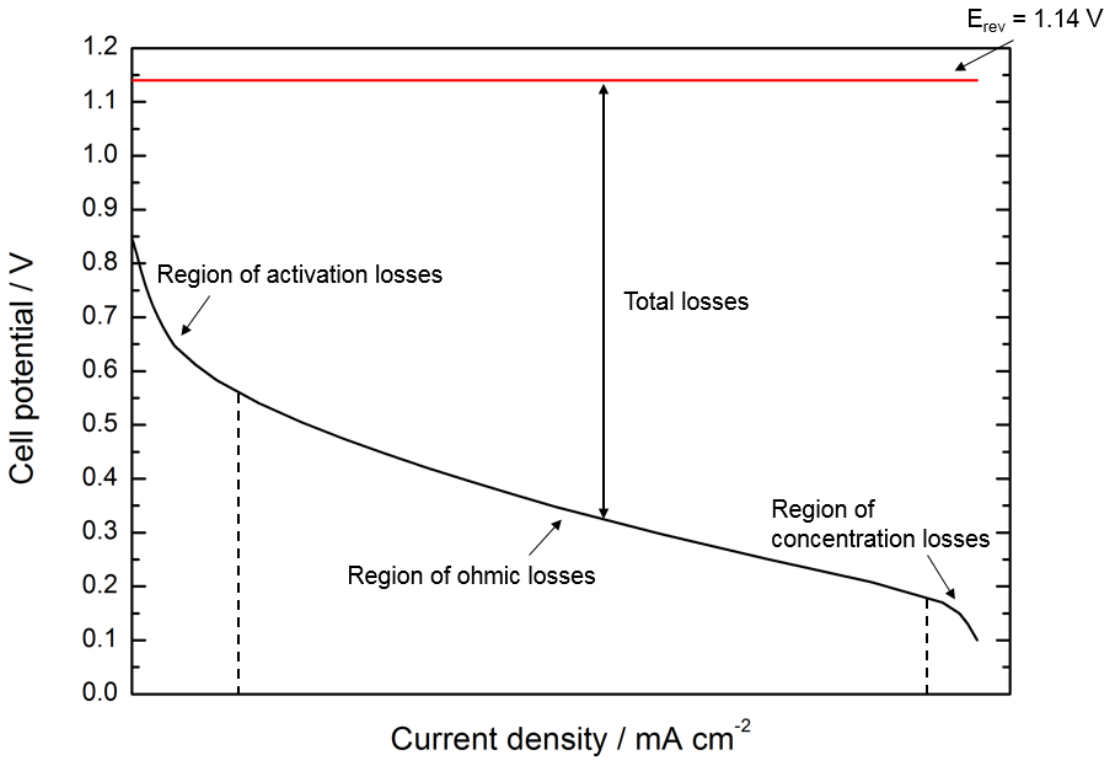

Figure 2-7: Polarization curve of an alkaline DEFC measurement and descriptions of the different characteristic regions in an U-I curve [38].

In the region of lower current densities, activation losses occur. The activation losses appear due to slow reaction kinetics at the electrodes, whereby an energy barrier has to be overcome so that electric and ionic current can flow. This process can be

compared to the activation energy of a chemical reaction. In this case, a certain amount of energy is needed to start the reaction which is often provided by heating up the reaction. In case of electrochemical reactions at the electrode surface, the activation is provided by voltage drops, also referred to as overpotentials. An overpotential describes the voltage that is needed at each electrode before the electrochemical reaction starts [38]. The total activation loss can be calculated according to Eq. 2-12.

$$\eta_{act} = \eta_a + \eta_c \qquad \text{Eq. 2-12}$$

η_{act} is the total activation loss and η_a and η_c are the overpotentials at the anode and cathode, respectively [30].

In the second region mainly ohmic losses are observed. The decreasing potential is directly proportional to the current density which can be described with Eq. 2-13:

$$\eta_{ohmic} = R_{cell} \cdot j \qquad \text{Eq. 2-13}$$

In Eq. 2-13, η_{ohmic} is the ohmic loss, R_{cell} the cell resistance and j the current density. The ohmic loss of a cell can be minimized when the distance between the electrodes is kept at a minimum and by improving the ionic conductivity of the electrolyte.

The concentration losses occur during the whole measurement, but appear more often at higher current densities as it becomes more difficult for the reactant to reach the active site of the catalyst. This loss is also more important for liquid reactants like ethanol compared to gaseous reactants like hydrogen. Reasons for concentration losses are a slow diffusion of the reactant to the active sites and also a slow diffusion of the product away from the active site. In general, concentration losses are more significant when the concentration of the reactants decreases and product accumulates or if the diffusion of those compounds is too slow [38].

3 Experimental

3.1 Materials and Methods

3.1.1 Chemicals

All chemicals were used like they were purchased without further purification.

- Carbon black Vulcan XC72R (Cabot Corporation)
- $PdCl_2$ anhydrous 59-60% Pd basis (Aldrich)
- $Ni(NO_3)_2 \cdot 6H_2O$ (Aldrich)
- $BiCl_3$, reagent grade, ≥98% (Aldrich)
- Polytetrafluoroethylene (PTFE) (Dupont)
- $(La_{0.8}Sr_{0.2})_{0.95}MnO_{3-x}$ (FuelCellMaterials)
- NaCl ≥99.5%, (Aldrich)
- HCl p.a. ≥ 32% (Fluka Analytics)
- $NaBH_4$ (Alfa Aesar)
- KOH 1.0 M Fixanal 1 L Ampoule (Sigma Aldrich)
- Ethanol absolute (EtOH abs., Sigma Aldrich)
- Ultrapure ~18 MΩ H_2O (Barnstead Nanopure Water Purification System)
- 2-Propanol ASC ≥ 99.8% (Sigma Aldrich)
- Nafion solution 5wt.% (Quintech)
- Alumina suspension, 0.05 µm (MasterPrep Bühler)
- Nitrogen, 5.0 (Air Liquide)
- Oxygen, 5.0 (Air Liquide)
- Carbon Cloth ELAT-H (FuelCellsEtc.)
- Toray Paper (FuelCellsEtc.)
- Polypropylene (PP) separator (Freudenberg 700/77)

3.1.2 Instruments

- Reference 600™ Potentiostat/Galvanostat/ZRA, GAMRY Instruments

- Rotating electrode (RDE710, GAMRY Instruments)
- RDE: Rotating disk electrode (glassy carbon area: 0.196 cm^2), Model AFE5T050GC, Pine Research Instrumentation
- RHE: reversible hydrogen electrode (gaskatel HydroFlex), Gaskatel Gesellschaft für Gassysteme durch Katalyse und Elektrochemie mbH
- Counter electrode: platinized titanium rod, Bank Elektronik – Intelligent controls GmbH
- Julabo, model MC, class: III, Julabo Labortechniken GmbH
- Ultrasonic bath (Elma/Elmasonic S 300)
- Scale: Sartorius BP 110S max. 110 g, Sartorius AG
- Magnetic stirrer: Heidolph MR Hei-Tech, Heidolph Instruments GmbH & Co. KG
- Drying oven: DRY-line, VWR#
- Hot press (Fontune Vlaardingen)
- Centrifuge: Labofuge 400, Heraeus
- Lab furnace: Jumo Dicon 501, Elsklo
- BaSyTec CTS (Cell Test System)
- Multiwave 3000 microwave system (Anton Paar)
- ICP-OES system: Arcos SOP by Spectro (Kleve, Germany)

3.2 Catalyst synthesis

The syntheses were carried out to obtain catalysts composed of 60wt.% carbon black (Vulcan XC72R) as support material and 40wt.% active metal catalyst material. The active material consisted of a molar ratio of x mol% palladium (Pd), y mol% nickel (Ni) and z mol% bismuth (Bi) expressed as: $Pd_xNi_yBi_z$.

Within the frame of this master's thesis, following catalysts were synthesized via simultaneous method ("instant method") where all metal precursors are mixed and deposited on the support material via reduction using $NaBH_4$: $Pd_{60}Ni_{40}$/C, $Pd_{60}Ni_{20}Bi_{20}$/C, $Pd_{70}Ni_{20}Bi_{10}$/C, $Pd_{40}Ni_{20}Bi_{40}$, $Pd_{70}Ni_{25}Bi_5$/C and $Pd_{80}Ni_{10}Bi_{10}$/C.

A glass vial was charged with the corresponding amount of $PdCl_2$, at least 2 eq. of NaCl and 10 mL of ultra-pure H_2O were added. NaCl is added because $PdCl_2$ is not soluble in ultra-pure H_2O but forms a water soluble, square-planar $[PdCl_4]^{2-}$ complex in the presence of additional chloride ions. Afterwards, the solution was sonicated for several hours until $PdCl_2$ was completely dissolved. $Ni(NO_3)_2 \cdot 6H_2O$ as well as $BiCl_3$ were put into glass vials and each dissolved in 10 mL ultra-pure H_2O. $BiCl_3$ does not dissolve in water but forms BiOCl which is insoluble. Therefore, some drops of HCl (37%) were added until all BiOCl was dissolved and a colorless clear solution was obtained.

The metal salt solutions were mixed. BiOCl started to precipitate again leading to clouding of the solution. Vulcan XC72R was suspended in 54 mL isopropyl alcohol (IPA) and 6 mL ultra-pure H_2O. The mixture was sonicated for 30 min before adding it to the metal salt solution. Afterwards, the pH was adjusted to 10-11 using 5.0 M NaOH. A freshly prepared reduction solution containing five eq. of $NaBH_4$ in 0.6 mL 1.0 M NaOH and 6 mL ultra-pure H_2O was added dropwise to the reaction mixture under stirring. Small bubble formation was observed, which indicates the reduction of the metal salts. Finally, the reaction mixture was heated up to 60 °C, stirred for four hours at 60 °C, allowed to cool to room temperature and stirred over-night at room temperature.

The following day, the product was obtained via centrifugation and was washed three times with ultra-pure H_2O. The resulting catalyst was dried in the drying cabined at 40 °C for at least two days.

3.3 ICP-OES measurement

The ICP-OES measurements were performed by Norbert Kienzl from Bioenergy 2020+ GmbH.

Metal concentrations of catalysts were determined by inductively coupled plasma optical emission spectrometry (ICP-OES) after microwave-assisted pressurized acid digestion.

A Multiwave 3000 microwave system was used for the digestion. About 5-10 mg of catalyst was mixed with 7 mL of concentrated nitric acid and 0.2 mL $HClO_4$ (Carl Roth, Karlsruhe, Germany). The temperature was ramped to 195 °C within 15 min with a power input of 1500 W, followed by a dwell time of 25 min at the maximum temperature. Finally, the samples were diluted to 25 mL with deionized water.

For the sample analysis following detection wavelengths were used: Bi 223.061 nm, Ni 231.604 nm, Pd 340.458 nm.

3.4 *Ex-situ* characterization

Each catalyst was characterized at least three times by cyclic voltammetry (CV) and chronoamperometry (CA) using a RDE set-up. The CV curves shown in chapter 4 represent the curve exhibiting the best performance. The mean value and the deviation for each catalytic parameter were calculated and are shown in additional tables.

For the *ex-situ* characterization of the catalysts, an ink for the application onto the GC electrode was prepared to obtain a concentration of 56 μg_{Pd} cm^{-2} on the RDE surface. Therefore, a glass vial was charged with the corresponding amount of catalyst, 1.75 mL isopropyl alcohol, 0.737 mL ultra-pure water and 13 µL of Nafion ionomer-solution as binder were added. The mixture was suspended for about 15 min in an ultrasonic ice bath. 5 µL of the slurry were applied on the GC electrode which was then rotated for about 10 min at 700 rpm. Afterwards, another 5 µL were applied and the RDE was rotated for about 30 min at 700 rpm until the catalyst material was dry.

For the CV/CA measurement, exactly 50 mL of 1.0 M KOH were filled into a glass cell, tempered at 30 °C and purged with nitrogen for 20-30 min. The measurement was carried out in a three-electrode assembly. A Reversible Hydrogen Electrode (RHE) as reference electrode and a platinized titanium rod as counter electrode were used.

Before the actual measurement, the internal resistance (IR) of the electrolyte was determined (5 Ω), but due to the low values no IR correction of the measured curves was performed.

First cleaning cycles were performed at a scan rate of 50 mV s^{-1} to remove impurities from the catalyst surface until a stable CV was obtained.

Then, CVs between 0.05 V–1.5 V and 0.05 V–1.2 V were recorded with following parameters:

- Scan rate: 10 mV s^{-1}
- Step size: 2 mV
- Number of cycles: at least 3 until stable CV is obtained

After CVs were recorded, 2.92 mL of absolute ethanol (EtOH) were added to 1.0 M KOH to obtain a solution with a concentration of approximately 1 M KOH and 1 M EtOH. The solution was purged with nitrogen for several minutes and the EOR was measured between 0.05 V and 1.2 V using the same parameters as described above.

Finally, a CA measurement was carried out. A potential of 0.83 V was applied for 3600 s and the current was measured.

3.5 *In-situ* characterization

The two catalysts with the best performance among all *ex-situ* characterized PdNiBi catalysts were tested in a single cell configuration and compared to the benchmark Pd/C. For the *in-situ* characterization, a single cell assembly with liquid electrolyte and a polypropylene (PP) separator was chosen. A galvanostatic measurement was carried out in which every step was held for 120 s. The last recorded value was used to create the polarization curve of the cell. Following currents were applied: 1 mA, 2 mA, 3 mA, 4 mA, 5 mA, 6 mA, 7 mA, 8 mA, 9 mA, 10 mA, 15 mA, 20 mA, 30 mA, 40 mA, 50 mA, 60 mA, 70 mA, 80 mA, 90 mA, 100 mA, 125 mA, 150 mA, 175 mA, 200 mA, 250 mA, 300 mA.

A mixture containing 6.0 M KOH and 1.0 M absolute ethanol was used as electrolyte. In order to record the anode potential during the measurement, a Luggin capillary was connected to the back of the anode. Before the cell measurement, the internal resistance in the single cell (around 0.5 Ω) was measured but no IR correction was performed.

3.5.1 Anode preparation

The anode was prepared by a drop coating according to Grimmer *et al.*. Resulting in a loading of 1 mg_{Pd} cm^{-2} and 30wt.% Nafion ionomer as binder on carbon cloth carrier material [39].

A glass vial was charged with Nafion solution (5wt.%) and 1.5 mL of n-propanol were added. The solution was sonicated for 30 min, the catalyst material was added along with another 0.5 mL of n-propanol and the mixture was sonicated again for 30 min. Four times 400 µL of the catalyst ink were applied dropwise on the carbon cloth piece (3×3 cm). After each application, the carbon cloth was dried in the drying cabinet at 40 °C for about 10 min. The anodes were kept in the drying cabinet overnight. The correct loading was ensured using gravimetric analysis.

3.5.2 Cathode preparation

The cathodes were prepared via cross-rolling according to Grimmer *et al.* [21] to result in a catalyst loading of 40-45 $mg_{catalyst}$ cm^{-2}. The cathode consisted of an active layer (AL) and a gas diffusion layer (GDL) which were prepared separately.

For the preparation of the AL, the perovskite-based catalyst $(La_{0.8}Sr_{0.2})_{0.95}MnO_{3-x}$, carbon black and polytetrafluoroethylene (PTFE) were mixed to result in a composition of 60wt.% catalyst, 20wt.% conductive material Vulcan XC72R and 20wt.% binder PTFE. About 10 mL of IPA:H_2O (1:1) were added and the mixture was stirred until a leathery dough was obtained. The GDL consisted of PTFE and acetylene black. Both the AL and the GDL were rolled separately until a thickness of 1.5 cm was reached for each layer. Afterwards, the GDL and the AL were rolled

together on the Nickel mesh (3×6 cm) until the electrode reached a total thickness of 2.2 cm.

The electrode was dry pressed twice between two filter papers at a pressure of 60-70 kg cm^{-2} and kept at 40 °C overnight. The following day, the cathode was put between two pieces of aluminum foil and two copper plates. The screws were tightened with torque of 6 N m. The electrodes were sintered at 330 °C for half an hour.

Before the single cell measurement, the cathode performance was tested in a half-cell to ensure its functionality. Therefore, the cathode was glued into the cathode compartment and measured in a tree-electrode assembly. As reference electrode a RHE and as counter electrode stainless steel were used. The RHE was connected via a Luggin capillary that was positioned approximately 2 mm away from the cathode. The compartment between the electrodes was filled with 6.0 M KOH. The cathode was kept in this assembly for five days. During that time, half-cell measurements as well as long term stability tests were performed at a BaSyTec CTS (Cell Test System) with an estimated O_2 flow of 20 mL min^{-1}.

3.5.3 Cell assembly

After the cathode half-cell test, the cell was disassembled to introduce the anode. The cathode compartment was used as tested before. The cathode was covered with a PP separator, followed by a Ni grid to ensure a good contact of the anode with the current collector. The anode was applied and covered with a graphite plate and a copper plate as current collector. A Luggin capillary was connected to the back of the anode compartment to follow the anode potential during the measurement.

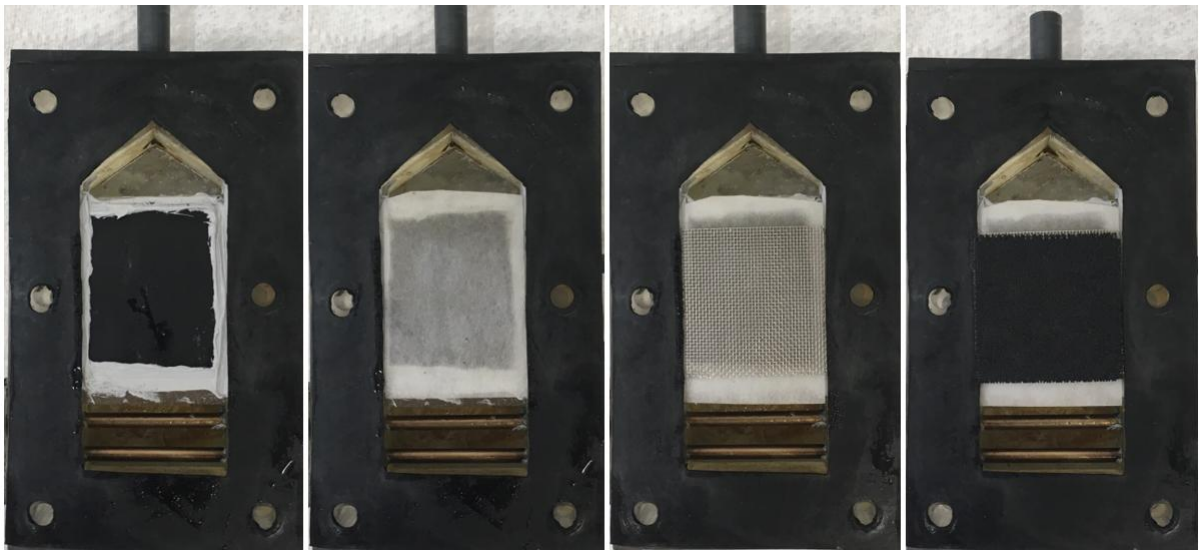

Figure 3-1: Cell assembly process from left to right: gluing in the cathode, applying the separator, the Ni mesh and the anode.

During the measurement, the anode compartment was supplied with a mixture containing 6.0 M KOH and 1.0 M EtOH as electrolyte (80 mL) at a flow rate of 10 mL min^{-1}. At the cathode compartment, oxygen was provided with an estimated flow rate of 20 mL min^{-1}. The cell measurement was performed at 30 °C.

4 Results and Discussion

The aim of this work is to investigate the influence of Ni and Bi on Pd-based catalysts and optimize the performance of the catalysts toward the EOR in alkaline medium by varying the atomic ratios of Pd, Ni and Bi. First, the influence of Ni and Bi was investigated by comparing the performance of PdNi/C, PdBi/C and PdNiBi/C catalysts in a RDE measurement to an in-house prepared Pd/C reference. As the PdNiBi/C catalyst showed promising results the Pd and Bi ratios were varied. After finding the best composition in terms of activity toward alkaline EOR, byproduct tolerance and stability, it was attempted to improve the performance even further by varying the Ni amount. All those catalysts were tested in a CV and a CA measurement. Finally, the best catalysts were tested in a single cell measurement and compared to Pd/C as reference material.

The results presented in chapter 4.1 and 4.3 are part of the publication: B. Cermenek, J. Ranninger, V. Hacker *et al.*, "Novel carbon supported ternary PdNiBi electrocatalyst for the alkaline ethanol oxidation reaction" Applied Catalysis B: Environmental, submitted 2017.

4.1 ICP-OES analysis

The ratio of carbon black to metals (calculated: 60wt.% of carbon black Vulcan XC72R and 40wt.% of metals) and also the composition of the metal alloy (x mol% Pd, y mol% Ni, z mol% Bi) of all synthesized catalysts were analyzed via an ICP-OES measurement.

Table 4-1: Results of the ICP-OES measurement.

Sample	Intended concentration / mol%			Measured concentration / mol%		
	Pd	Ni	Bi	Pd	Ni	Bi
Pd/C	1	-	-	1	-	-
$Pd_{60}Ni_{40}/C$	0.60	0.40	-	0.60	0.40	-
$Pd_{60}Bi_{40}/C$	0.60	-	0.40	0.61	-	0.39
$Pd_{60}Ni_{20}Bi_{20}/C$	0.60	0.20	0.20	0.61	0.19	0.20
$Pd_{70}Ni_{20}Bi_{10}/C$	0.70	0.20	0.10	0.70	0.19	0.11
$Pd_{40}Ni_{20}Bi_{40}/C$	0.40	0.20	0.40	0.46	0.17	0.37
$Pd_{70}Ni_{25}Bi_{5}/C$	0.70	0.25	0.05	0.71	0.25	0.05
$Pd_{80}Ni_{10}Bi_{10}/C$	0.80	0.10	0.10	0.78	0.10	0.12

The ICP-OES results show that the intended metal content is very close to the measured concentrations (see Table 4-1).

4.2 *Ex-situ* characterization

For the *ex-situ* measurement, exactly 56 μg_{Pd} cm^{-2} are applied on the GC electrode to ensure comparable results. Not only the amount but also the distribution of the catalyst on the electrode plays an important role. In former experiments, a glass vial was charged with the corresponding amount of catalyst and 1.75 mL of IPA and 0.75 mL of ultra-pure water were added. The mixture was sonicated for 10 min. Afterwards, 5 µL of the catalyst ink were transferred on the GC and rotated with a rotation speed of 700 rpm for 15 min. Subsequently, another 5 µL of the ink were applied and the electrode was rotated with the same speed for 30 min. The result was often an uneven distribution of the catalyst. Furthermore, the catalyst was often flaking off during the measurement and the procedure had to be repeated.

Shinozaki *et al.* compared ink formulations for the RDE measurement with and without Nafion ionomer. They prepared a statistically significant number of catalyst inks and compared the EASA, mass activity and the specific mass activity of the different ink formulations in RDE measurements. It was found that the measurements using Nafion in the ink did not exhibit the highest activity, as the catalyst film thickness is higher than in Nafion-free inks but the results were better in respect to

reproducibility. The better reproducibility originates from a better dispersion of the catalyst. The optimal dispersion of catalyst particles in the ink is obtained at a concentration of 24wt.% Nafion. It was also reported that the temperature of the catalyst slurry rises upon sonication which leads to a significantly lower EASA due to thermally induced degradation of smaller catalyst particles. This effect can be reduced by putting the catalyst ink in ice-water bath during the sonication process [40].

Pollet *et al.* studied the influence of the sonication parameters on the distribution of Pt nanoparticles in catalyst inks. They found that the frequency and power of the sonication bath or probe are essential. Again the EASA was used to compare the different catalyst ink formulations. It was found that the EASA of the ink sonicated for 120 min decreased by 45% compared to the sample sonicated only for 30 min. They stated that sonication is important to distribute the Nafion binder between the nanoparticles, but after longer sonication time Nafion is separated again and nanoparticle agglomeration as well as Pt dissolution occurs [41].

The composition of the catalyst ink for the RDE measurement was then changed to catalyst, 1.75 mL IPA, 0.737 mL ultra-pure H_2O and 13 µL of Nafion ionomer solution. Furthermore, the catalyst ink was sonicated only for 15 min in an ice-bath. The application and drying procedure was not changed. Improvements in the catalyst particle dispersion in the ink and in the distribution of the catalyst on the RDE were observed.

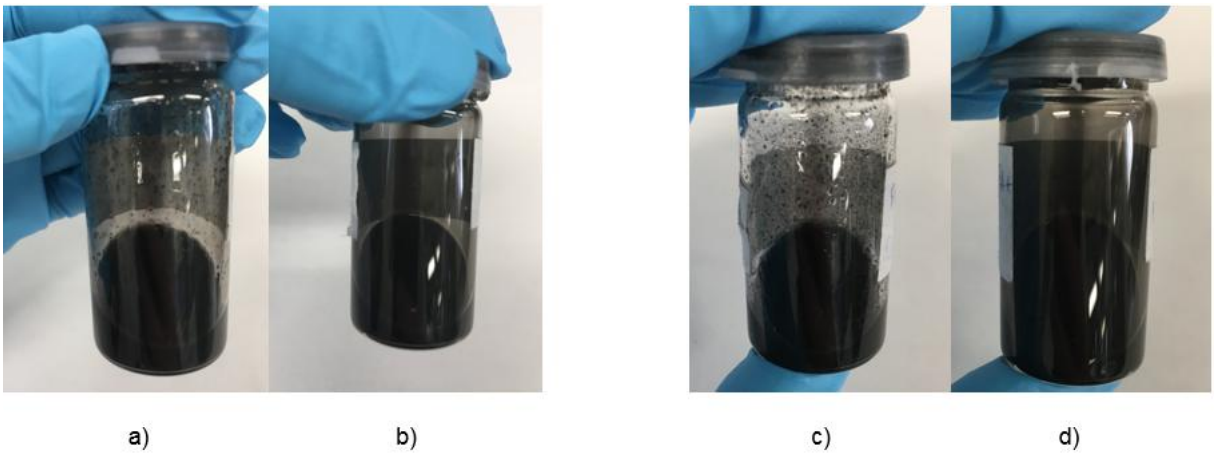

Figure 4-1: Influence of sonication temperature (a) without ice-water bath, b) with ice-water bath) and influence of Nafion (c) ink without Nafion and d) ink with Nafion) on the dispersion of the catalyst particles in the ink for RDE measurement.

Figure 4-1 shows the influence of the sonication temperature and the addition of small amounts of Nafion on the particle distribution in the catalyst ink. In a), the catalyst ink was sonicated without an ice-water bath, whereas the catalyst ink in b) was sonicated in an ice bath. In slurry a) bigger particles are visible on the glass surface whereas slurry b) seems to have a homogeneous composition. The same phenomenon can be observed when investigating the influence of Nafion. The catalyst ink c) is prepared without Nafion and shows bigger particles, whereas slurry d) with Nafion is homogenous.

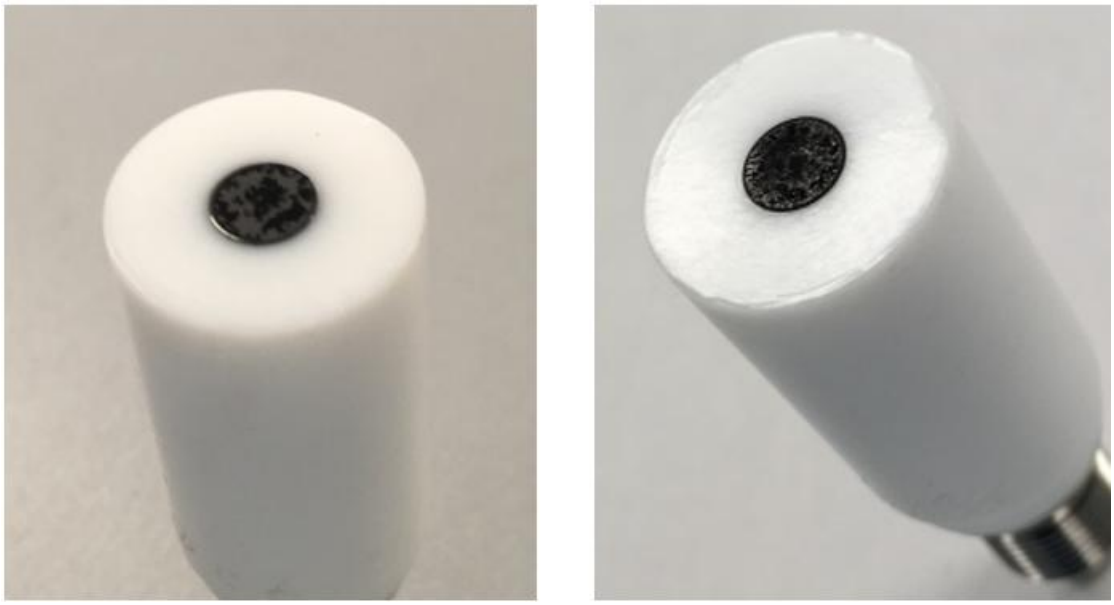

Figure 4-2: Distribution of the catalyst material on the RDE without Nafion (left) and with Nafion (right).

The positive influence of Nafion ionomer in the catalyst ink can also be observed in the homogeneous distribution on the RDE. Only some areas of the GC are covered with catalyst in the Figure 4-2 (left) (catalyst ink without Nafion ionomer). In the Figure 4-2 (right), on the other hand a more homogeneous distribution is obtained, when adding Nafion ionomer solution to the ink. Applying the improved RDE ink preparation procedure, it was observed that flaking off of the catalyst during the measurement was prevented and reproducible results were obtained.

4.3 The influence of Ni and Bi on Pd/C catalysts

In order to study the influence of Ni and Bi on Pd/C catalyst, the catalysts $Pd_{60}Ni_{40}$/C and $Pd_{60}Ni_{20}Bi_{20}$/C were synthesized and compared in a RDE measurement to Pd/C and $Pd_{60}Bi_{40}$/C as two in-house prepared references.

4.3.1 Cyclic voltammetry

Figure 4-3 shows the CVs of the Pd/C, $Pd_{60}Ni_{40}$/C, $Pd_{60}Bi_{40}$/C and $Pd_{60}Ni_{20}Bi_{20}$/C catalysts in 1.0 M KOH. When comparing Pd/C with $Pd_{60}Ni_{40}$/C, the curves look similar only the peaks are less distinct for $Pd_{60}Ni_{40}$/C. Obradović *et al.* investigated a Ni electrode in a CV measurement. They found in a recorded CV between the potentials -1.5 V and 0.5 V vs. RHE characteristic peaks in the anodic scan at 0.3 V and in the cathodic scan at -0.5 V. The peaks were attributed to the formation and reduction of Ni → α-$Ni(OH)_2$. In a second CV measured between the potential 0.1 V and 1.5 V vs. RHE, the former mentioned peaks disappeared. New peaks at 1.35 V and 1.48 V appeared. Those peaks are matched to the reaction of Ni(II) species which form NiOOH at potentials higher than 1.3 V. It was also stated that in a CV recorded from -0.2 V to 1.2 V no peaks were observed which is explained with transformation of α-$Ni(OH)_2$ at lower potentials to β-$Ni(OH)_2$ at higher potentials. β-$Ni(OH)_2$ cannot be reduced when reversing the potential which explains the absence of peaks [42].

From these findings, it is plausible that the CV curve of the Pd/C and $Pd_{60}Ni_{40}$/C catalyst are similar within the chosen potential range, as the peaks in the $Pd_{60}Ni_{40}$/C only originate from Pd.

The comparison of the Pd/C with $Pd_{60}Bi_{40}$/C catalyst shows more differences in the CV curves. First of all, the peaks between 0.05 V and 0.4 V vs. RHE, corresponding to the adsorption/desorption of hydrogen, basically disappear (see Figure 4-3). Simões *et al.* reported that Bi hinders the absorption of hydrogen into the Pd lattice leading to no observable peaks in this potential region [43]. The other difference between the CV of Pd/C and $Pd_{60}Bi_{40}$/C catalyst is the occurring peak in the anodic

scan at around 0.9 V. Casella *et al.* suggested the formation of bismuth oxide species according to reaction (8) [44]:

$$2\ Bi + 6\ OH^- \rightarrow Bi_2O_3 + 3\ H_2O + 6\ e^- \qquad (8)$$

Simões *et al.* stated that the Bi_2O_3 is present as $Bi(OH)_3$ in aqueous medium and not soluble in alkaline solutions. The reduction of Bi oxide species like the reduction of Pd oxide species is observable in the cathodic sweep at 0.7 V [43].

If not only the reduction of PdO species but also BiO species occurs at the same potential, the calculation of the EASA as described in section 2.4.2 does not give representative results anymore. The EASAs were still calculated as described above under the assumption that the peak for the reduction of BiO and PdO species do not overlay. (see Table 4-2 and Figure 4-4).

In the CV of $Pd_{60}Ni_{20}Bi_{20}/C$, the peak which is attributed to the Bi oxide film formation as well as the reduction peak at 0.7 V are dramatically increased. In particular, the EASA calculated from the PdO reduction peak more than doubles compared to Pd/C (see Figure 4-4), even though less Bi is added to the catalyst than in the $Pd_{60}Bi_{40}/C$. Neto *et al.* described a study on PdBi/C catalysts with different atomic ratios and found the more Bi is added the more agglomerations are formed which block the active sites of the Pd and decrease the activity of the catalyst [27]. The suppression of the hydrogen absorption/ desorption processes is still observed when only 20% of Bi are added.

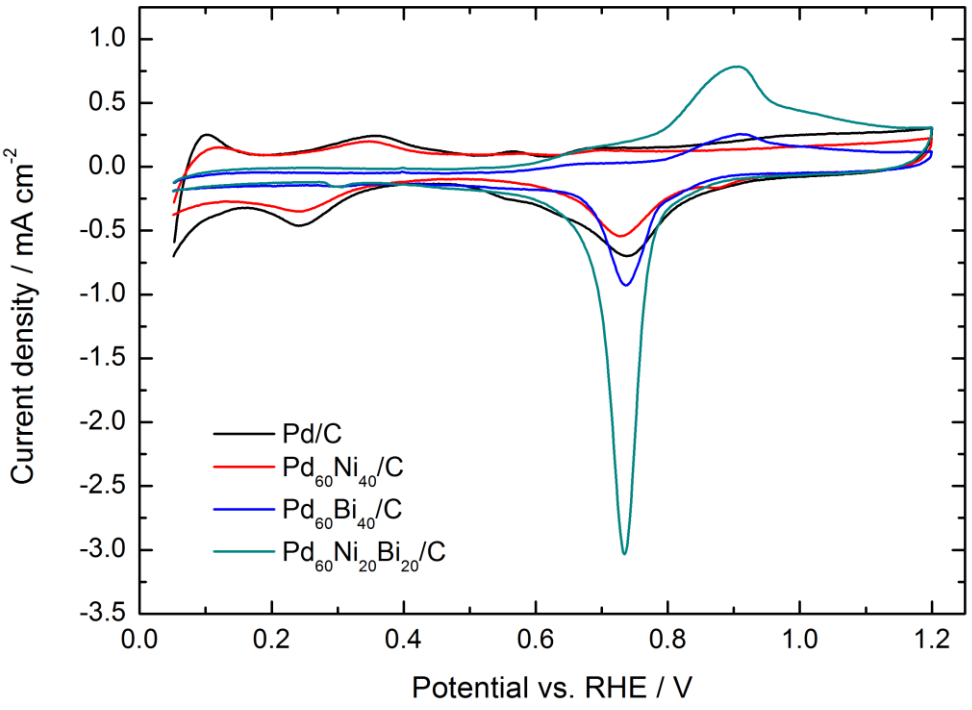

Figure 4-3: CVs of Pd/C, $Pd_{60}Ni_{40}$/C, $Pd_{60}Bi_{40}$/C and $Pd_{60}Ni_{20}Bi_{20}$/C catalysts, recorded in 1.0 M KOH at 30 °C with a scan rate of 10 mV s^{-1}.

Table 4-2: EASAs of Pd/C, $Pd_{60}Ni_{40}$/C, $Pd_{60}Bi_{40}$/C and $Pd_{60}Ni_{20}Bi_{20}$/C catalysts, calculated from CVs recorded in 1.0 M KOH at 30 °C with a scan rate of 10 mV s^{-1}.

Catalyst	EASA mg cm^{-2}		Standard deviation mg cm^{-2}
Pd/C	463.2	±	78.4
$Pd_{60}Ni_{40}$/C	338.6	±	48.6
$Pd_{60}Bi_{40}$/C	275.6	±	22.3
$Pd_{60}Ni_{20}Bi_{20}$/C	983.2	±	34.5

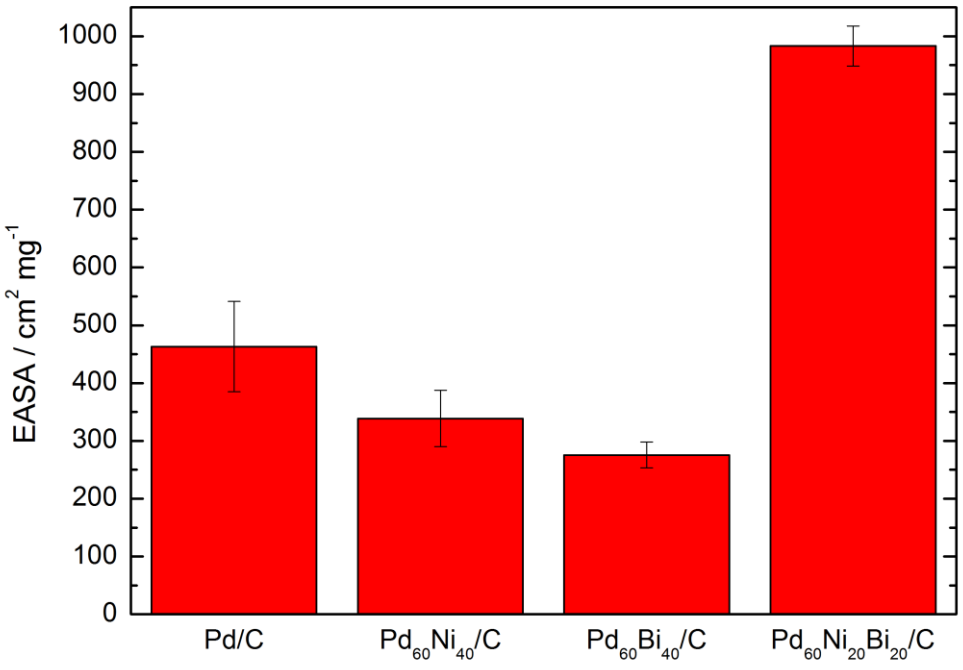

Figure 4-4: EASAs of Pd/C, $Pd_{60}Ni_{40}$/C, $Pd_{60}Bi_{40}$/C and $Pd_{60}Ni_{20}Bi_{20}$/C catalysts, calculated from the CVs recorded in 1.0 M KOH at 30 °C with a scan rate of 10 mV s^{-1}.

4.3.2 Ethanol Oxidation Characteristics

After the CV was measured in 1.0 M KOH solution and the EASA was calculated, 2.92 mL of absolute ethanol were added to obtain a solution with a concentration of approximately 1 M KOH and 1 M EtOH.

From the CVs recorded in an aqueous solution containing 1 M KOH and 1 M EtOH (see Figure 4-5), it is observed that the addition of Ni to Pd increases the peak current density by more than 20%. The onset potentials of Pd/C and $Pd_{60}Ni_{40}$/C catalysts are similar with 0.28 V and 0.29 V, respectively (see Figure 4-5 and Table 4-3). However, Zhang *et al.* and Dutta *et al.* found that compositions containing more than 40% Ni are more active toward the EOR in alkaline medium. From their results a Ni content between 50 and 70% leads to the best performance of the catalyst [30,42]. The onset potential of Bi containing catalysts is shifted to higher potentials and the peak current density is also decreased. The onset potential and the peak current

density of the $Pd_{60}Ni_{20}Bi_{20}/C$ catalyst are better compared to $Pd_{60}Bi_{40}/C$ which can be explained with the presence of Ni, but is also in accordance with the findings of Neto *et al.* who stated that lower amounts of Bi improve the activity more (see Figure 4-5 and Table 4-3) [27].

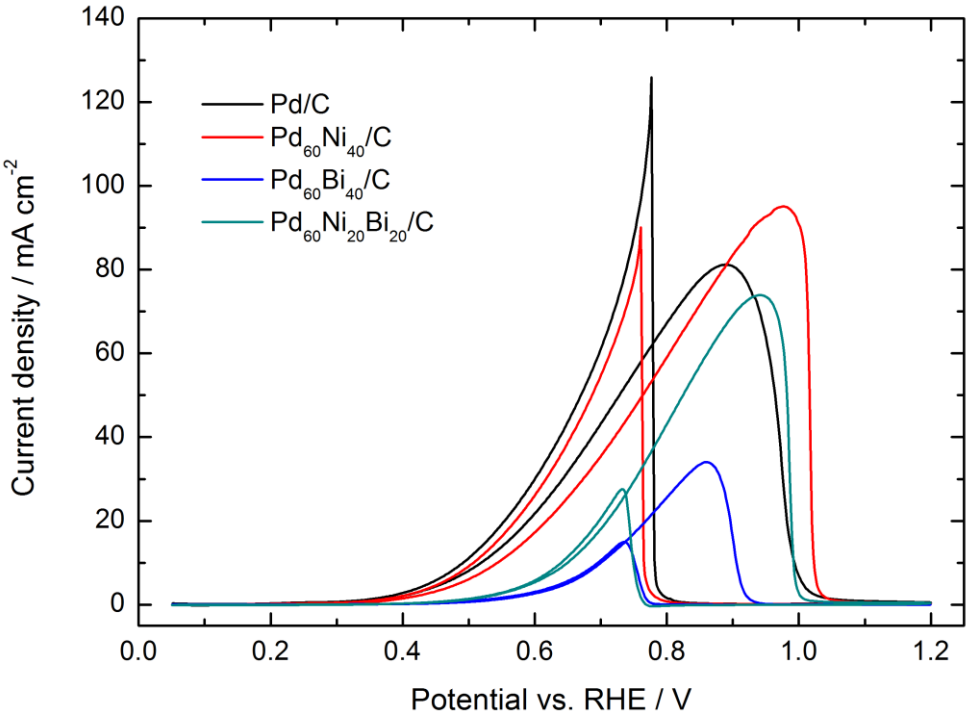

Figure 4-5: CVs of Pd/C, $Pd_{60}Ni_{40}/C$, $Pd_{60}Bi_{40}/C$ and $Pd_{60}Ni_{20}Bi_{20}/C$ catalysts, recorded in an aqueous solution (1 M KOH and 1 M EtOH) at 30 °C with a scan rate of 10 mV s^{-1}.

Table 4-3: Onset potentials and peak current densities of Pd/C, $Pd_{60}Ni_{40}/C$, $Pd_{60}Bi_{40}/C$ and $Pd_{60}Ni_{20}Bi_{20}/C$ catalysts recorded in an aqueous solution (1 M KOH and 1 M EtOH) at 30 °C with a scan rate of 10 mV s^{-1}.

Catalyst	Onset potential V		Standard deviation V	Peak current density mA cm^{-2}		Standard deviation mA cm^{-2}
Pd/C	0.280	±	0.015	78.6	±	9.8
$Pd_{60}Ni_{40}/C$	0.290	±	0.018	96.0	±	10.4
$Pd_{60}Bi_{40}/C$	0.352	±	0.015	37.6	±	3.1
$Pd_{60}Ni_{20}Bi_{20}/C$	0.348	±	0.007	65.5	±	7.6

Even though the activities of $Pd_{60}Ni_{20}Bi_{20}/C$ and $Pd_{60}Bi_{40}/C$ are lower than of Pd/C and $Pd_{60}Ni_{40}/C$, the very low peak current density in the cathodic sweep for the Bi containing catalysts indicates a very good byproduct tolerance (see Figure 4-6). The byproduct tolerances of the catalysts are calculated using the peak currents as well as the areas (total charge) of the peaks. The value for the byproduct tolerance of $Pd_{60}Ni_{20}Bi_{20}/C$ calculated from the peak areas is almost 200% higher than the byproduct stability of Pd/C (see Table 4-4). Paschos *et al.* researched PdBi catalysts in a CO stripping experiment and found that one Bi atom blocks 3 Pd atoms and avoids the poisoning of the active sites. It was also found that temperature treatment around 300 °C leads to a better alloying of Bi with Pd and higher activity [46].

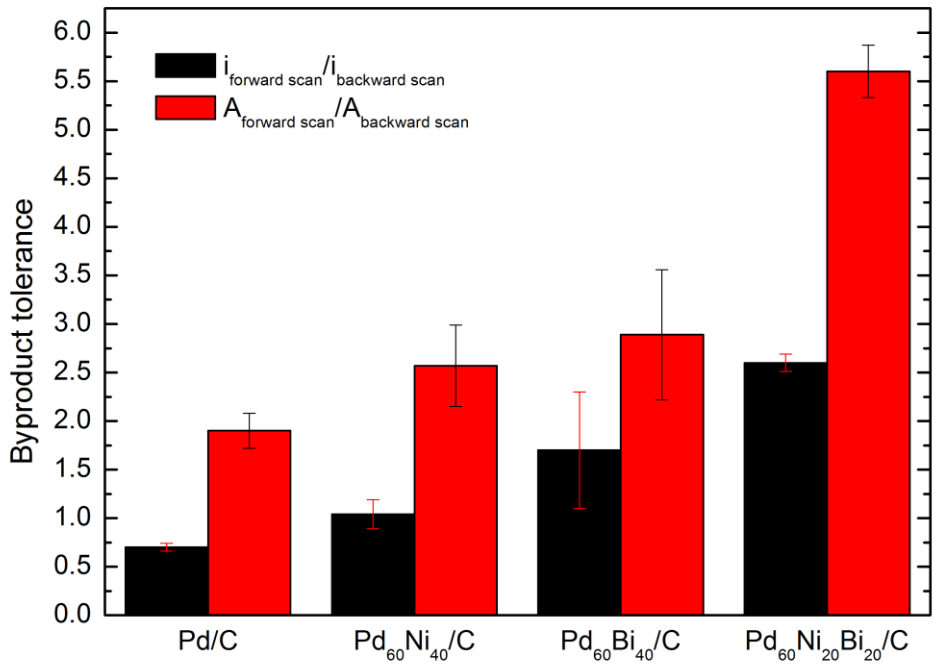

Figure 4-6: Byproduct tolerances of Pd/C, $Pd_{60}Ni_{40}/C$, $Pd_{60}Bi_{40}/C$ and $Pd_{60}Ni_{20}Bi_{20}/C$ catalysts, calculated from the peak currents and peak areas, from the CVs recorded in an aqueous solution (1 M KOH and 1 M EtOH) at 30 °C with a scan rate of 10 mV s^{-1}.

Table 4-4: Byproduct tolerances calculated from the peak currents and peak areas of Pd/C, $Pd_{60}Ni_{40}$/C, $Pd_{60}Bi_{40}$/C and $Pd_{60}Ni_{20}Bi_{20}$/C catalysts, from the CVs recorded in an aqueous solution (1 M KOH and 1 M EtOH) at 30 °C with a scan rate of 10 mV s^{-1}.

Catalyst	$i_{forward\ scan}$/ $i_{backward\ scan}$		Standard deviation	$A_{forward\ scan}$/ $A_{backward\ scan}$		Standard deviation
Pd/C	0.70	±	0.04	1.90	±	0.18
$Pd_{60}Ni_{40}$/C	1.04	±	0.15	2.57	±	0.42
$Pd_{60}Bi_{40}$/C	1.70	±	0.60	2.89	±	0.67
$Pd_{60}Ni_{20}Bi_{20}$/C	2.60	±	0.09	5.60	±	0.27

4.3.3 Chronoamperometry performance

After the CV measurements, a CA measurement was performed at a potential of 0.83 V for one hour. The CA measurement is an indication for the stability of the catalyst. $Pd_{60}Ni_{20}Bi_{20}$/C shows the best stability of all tested catalysts. The curve of $Pd_{60}Ni_{20}Bi_{20}$/C is flat shaped while e.g. the curve of $Pd_{60}Ni_{40}$/C is rather steep indicating a fast degradation of the catalyst (see Figure 4-7). It is worth mentioning that the potential that is chosen for the CA measurement is crucial for the performance of the catalyst during this test. The potential has to be below the peak potential and above the onset potential, however, for each catalyst another potential would be ideal but one potential has to be chosen to be able to compare the results. In case of $Pd_{60}Bi_{40}$/C the peak potential is around 0.83 V and only one reasonable curve was recorded as in the other curves, the current density decreased too fast because 0.83 V was too close to the peak potential. The potential of 0.83 V for the CA measurement was used in previous measurements and suitable for every catalyst except for $Pd_{60}Bi_{40}$/C. In respect to comparability, the potential was not changed upon that result.

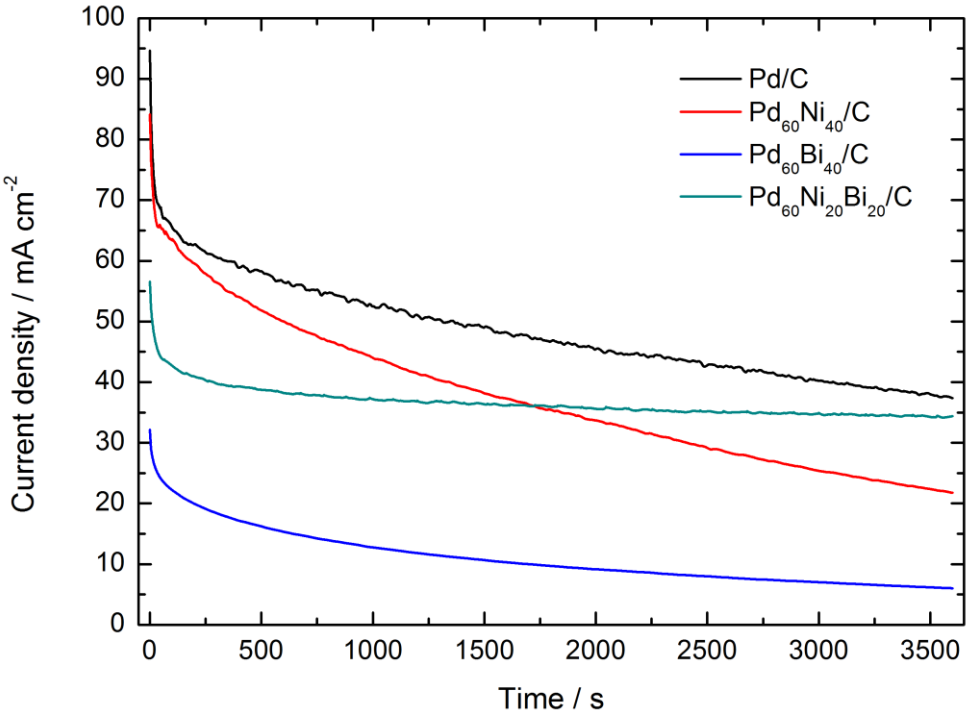

Figure 4-7: CA curves of Pd/C, $Pd_{60}Ni_{40}$/C, $Pd_{60}Bi_{40}$/C and $Pd_{60}Ni_{20}Bi_{20}$/C catalysts at 0.83 V vs. RHE in an aqueous solution (1 M KOH and 1 M EtOH) at 30 °C.

To compare the results of the CA measurements, the remaining current density of the catalysts after one hour was calculated and compared.

Table 4-5: Calculated remaining current densities of Pd/C, $Pd_{60}Ni_{40}$/C, $Pd_{60}Bi_{40}$/C and $Pd_{60}Ni_{20}Bi_{20}$/C catalysts after one hour of CA measurement at 0.83 V vs. RHE in an aqueous solution (1 M KOH and 1 M EtOH) at 30 °C.

Catalyst	Remaining current density after 3600 s %		Standard deviation %
Pd/C	33.0	±	8.4
$Pd_{60}Ni_{40}$/C	19.4	±	5.6
$Pd_{60}Bi_{40}$/C	18.7	±	-
$Pd_{60}Ni_{20}Bi_{20}$/C	55.3	±	11.18

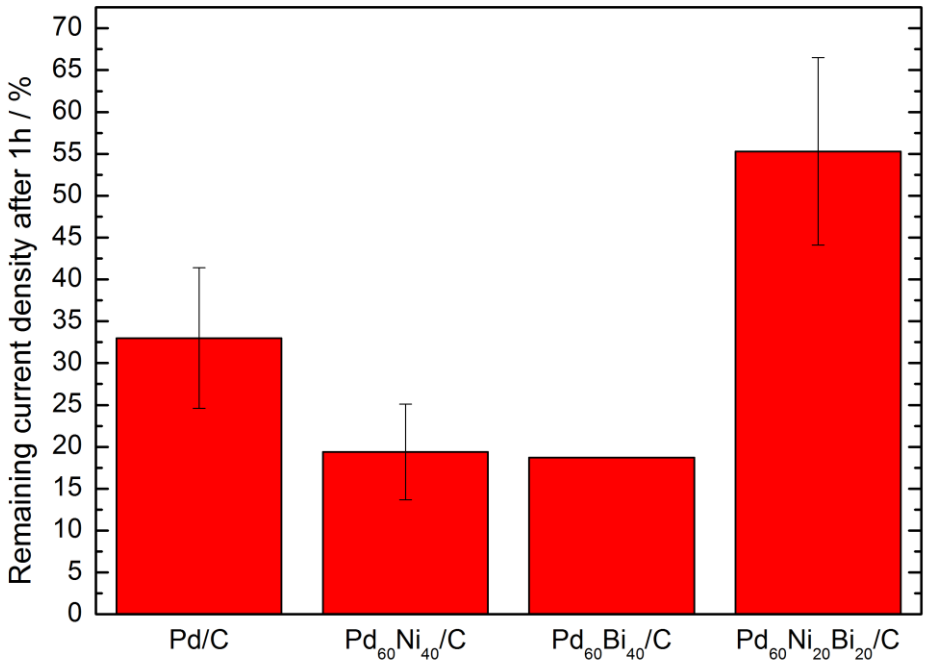

Figure 4-8: Remaining current densities of Pd/C, $Pd_{60}Ni_{40}$/C, $Pd_{60}Bi_{40}$/C and $Pd_{60}Ni_{20}Bi_{20}$/C catalysts after one hour of CA measurement at 0.83 V vs. RHE in an aqueous solution (1 M KOH and 1 M EtOH) at 30 °C.

The results of the CA measurement show that the stability of the $Pd_{60}Ni_{20}Bi_{20}$/C catalyst is far better than of the other catalysts (see Figure 4-8 and Table 4-5). The high stability of the $Pd_{60}Ni_{20}Bi_{20}$/C catalyst correlates with a high byproduct stability of this catalyst. If less poisonous species are accumulated at the catalyst it can be assumed that the catalyst is also more stable. However, the correlation between byproduct tolerance and stability was not found for the other tested catalysts. Considering the high byproduct tolerance and the high stability obtained from the *ex-situ* measurements, the $Pd_{60}Ni_{20}Bi_{20}$/C catalyst is a promising candidate for the application as anode catalyst in the alkaline DEFC.

4.4 Variation of the Pd and Bi content

Neto *et al.* found that the activity of Pd-based catalysts improves when only small amounts of Bi are added [27]. Tusi *et al.* confirmed those results and stated that for Pt-based catalysts, the phenomenon is reversed. The activities of Pt-based catalysts is found to be enhanced with increasing Bi amount [47]. To investigate the influence of the Bi ratio on the PdNi/C catalyst, the catalysts $Pd_{40}Ni_{20}Bi_{40}$/C and $Pd_{70}Ni_{20}Bi_{10}$/C were synthesized and compared to $Pd_{60}Ni_{20}Bi_{20}$/C. $Pd_{60}Ni_{40}$/C was also used as a benchmark in the measurements because this catalyst showed the highest activity in the previous experiments.

4.4.1 Cyclic voltammetry

The CV of the $Pd_{70}Ni_{20}Bi_{10}$/C catalyst exhibits a peak in the region between 0.1 and 0.2 V indicating an occurring hydrogen sorption reaction (see Figure 4-9). The Bi content in this catalyst appears to be too low to suppress the hydrogen sorption reaction completely. It is also noticed that in CVs of catalysts containing more than 10% Bi ($Pd_{60}Ni_{20}Bi_{20}$/C and $Pd_{40}Ni_{20}Bi_{40}$/C), an additional peak in the anodic sweep between 0.6 and 0.7 V is observed (see Figure 4-9) which was also found by Neto *et al.* [27].

In EDX experiments, Simões *et al.* found Bi^0-agglomerates in catalysts with a Bi content as high as 20% or higher. However, these agglomerations were not found in catalysts with a lower Bi ratio. These authors also stated that the peak at 0.9 V in the anodic sweep depends on the Bi concentration. The higher the Bi content of the catalyst the higher is this peak [43]. These results could not be confirmed in these experiments. In this study, the peak at 0.9 V of $Pd_{40}Ni_{20}Bi_{40}$/C is lower than the peak for $Pd_{60}Ni_{20}Bi_{20}$/C (see Figure 4-9). In the CV measurements of the $Pd_{40}Ni_{20}Bi_{40}$/C catalyst, many cleaning cycles had to be performed until a stable CV was obtained, because the peaks continued to decrease. A decreasing peak can indicate the presence of impurities which undergo an oxidative removal or other species that are dissolved with increasing potential. As this phenomenon was only observed in $Pd_{60}Bi_{40}$/C and $Pd_{40}Ni_{20}Bi_{40}$/C, it is assumed that the Bi^0-agglomerates, mentioned by Simões *et al.*, are oxidized and dissolved into the electrolyte. This thesis is

supported by the observation that the current in the EOR measurement of $Pd_{60}Bi_{40}/C$ and $Pd_{40}Ni_{20}Bi_{40}/C$ increased when more cycles were performed. Bi^0-agglomerates which also block the active sites of Pd are gradually dissolved and lead to a higher activity after multiple CV cycles.

The EASA of the $Pd_{60}Ni_{20}Bi_{20}/C$ catalyst is the highest among the tested catalysts. The $Pd_{70}Ni_{20}Bi_{10}/C$ catalyst exhibits the second highest EASA (see Table 4-6 and Figure 4-10). These results are conclusive in respect of the findings of Simões *et al.*, that the reduction peak at 0.7 V not only originates from Pd oxide species but also other oxidized species are reduced in this region [43]. As more Bi is incorporated in the $Pd_{60}Ni_{20}Bi_{20}/C$ catalyst and more Bi species can be oxidized, the reduction peak at 0.7 V in the cathodic sweep is also more distinct compared to $Pd_{70}Ni_{20}Bi_{10}/C$. The EASA of the $Pd_{40}Ni_{20}Bi_{40}/$ is assumed to be lower due to the low Pd content and the high Bi content leading to agglomerations.

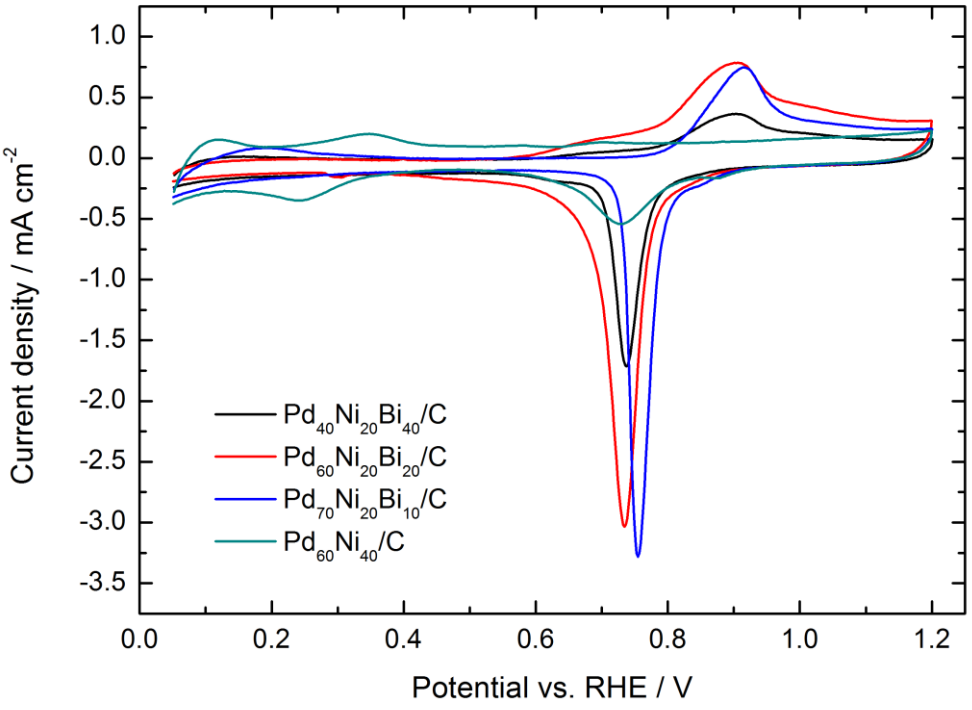

Figure 4-9: CVs of $Pd_{40}Ni_{20}Bi_{40}/C$, $Pd_{60}Ni_{20}Bi_{20}/C$, $Pd_{70}Ni_{20}Bi_{10}/C$ and $Pd_{60}Ni_{40}/C$ catalysts recorded in 1.0 M KOH at 30 °C with a scan rate of 10 mV s^{-1}.

Table 4-6: EASAs of $Pd_{40}Ni_{20}Bi_{40}/C$, $Pd_{60}Ni_{20}Bi_{20}/C$, $Pd_{70}Ni_{20}Bi_{10}/C$ and $Pd_{60}Ni_{40}/C$ catalysts calculated from the CVs recorded in 1.0 M KOH at 30 °C with a scan rate of 10 mV s^{-1}.

Catalyst	EASA mg cm^{-2}		Standard deviation mg cm^{-2}
$Pd_{40}Ni_{20}Bi_{40}/C$	421.0	±	51.7
$Pd_{60}Ni_{20}Bi_{20}/C$	983.2	±	34.5
$Pd_{70}Ni_{20}Bi_{10}/C$	549.3	±	71.5
$Pd_{60}Ni_{40}/C$	338.6	±	48.6

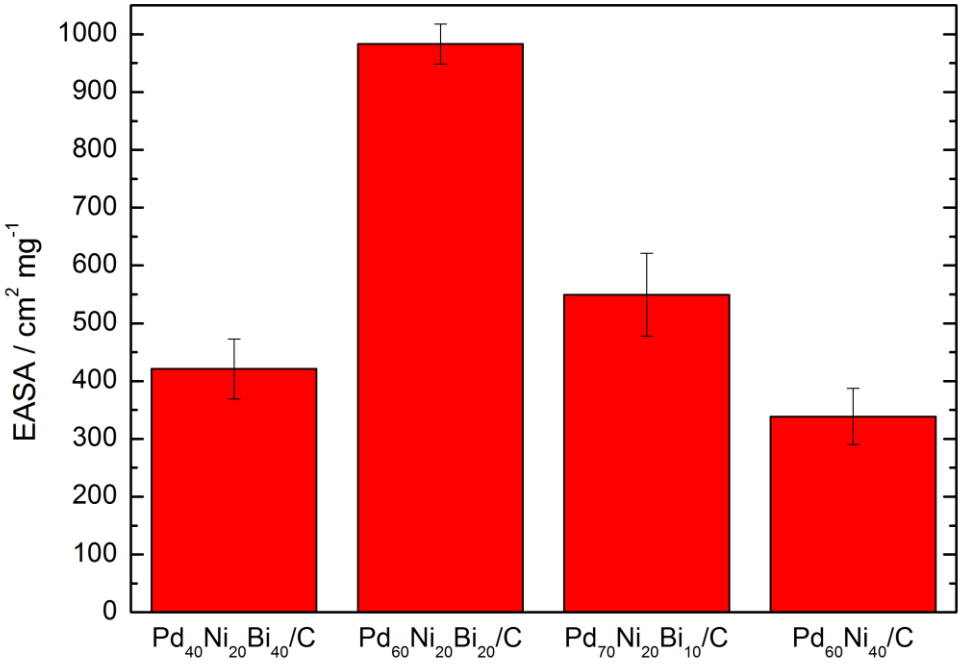

Figure 4-10: EASAs of $Pd_{40}Ni_{20}Bi_{40}/C$, $Pd_{60}Ni_{20}Bi_{20}/C$, $Pd_{70}Ni_{20}Bi_{10}/C$ and $Pd_{60}Ni_{40}/C$ catalysts, calculated from the CVs recorded in 1.0 M KOH at 30 °C with a scan rate of 10 mV s^{-1}.

4.4.2 Ethanol Oxidation Characteristics

The $Pd_{70}Ni_{20}Bi_{10}/C$ catalyst exceeded the performance of $Pd_{60}Ni_{40}/C$ in terms of peak current density and onset potential (see Figure 4-11). The onset potential for the EOR was decreased by 54 mV using the $Pd_{70}Ni_{20}Bi_{10}/C$ and the peak current density could be increased by 10 mA cm^{-2} compared to $Pd_{60}Ni_{40}/C$ (see Table 4-7). This result proofs that small amounts of Bi in the catalyst enhance the activity and kinetics toward the EOR in alkaline media.

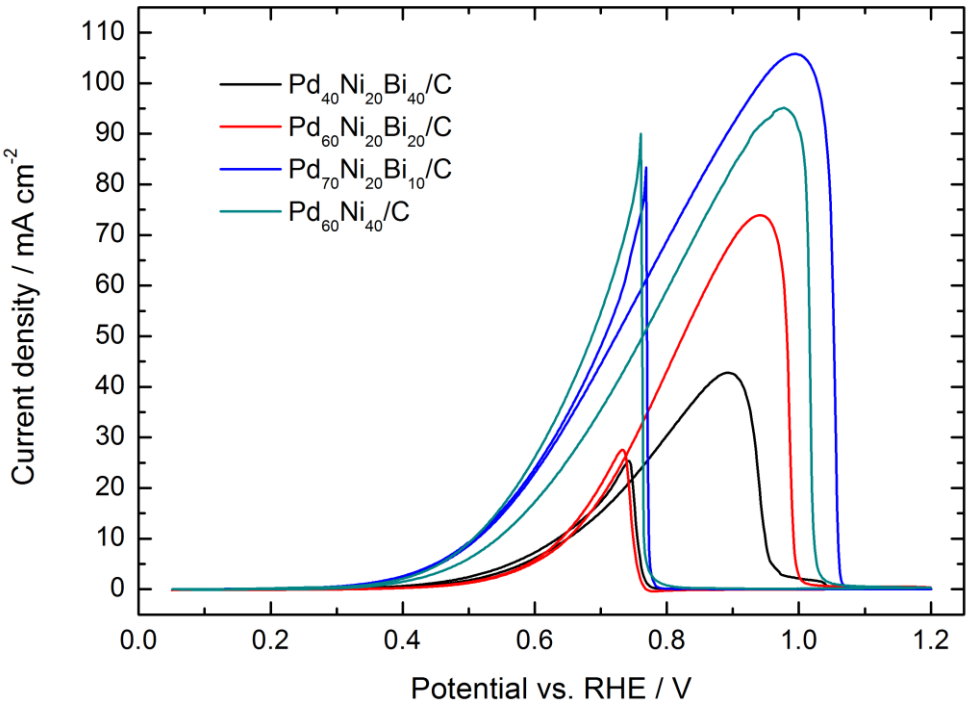

Figure 4-11: CVs of $Pd_{40}Ni_{20}Bi_{40}/C$, $Pd_{60}Ni_{20}Bi_{20}/C$, $Pd_{70}Ni_{20}Bi_{10}/C$ and $Pd_{60}Ni_{40}/C$ catalysts recorded in an aqueous solution (1 M KOH and 1 M EtOH) at 30 °C with a scan rate of 10 mV s^{-1}.

Table 4-7: Onset potentials and peak current densities of $Pd_{40}Ni_{20}Bi_{40}$/C, $Pd_{60}Ni_{20}Bi_{20}$/C, $Pd_{70}Ni_{20}Bi_{10}$/C and $Pd_{60}Ni_{40}$/C catalysts in an aqueous solution (1 M KOH and 1 M EtOH).

Catalyst	Onset potential V		Standard deviation V	Peak current density mA cm^{-2}		Standard deviation mA cm^{-2}
$Pd_{40}N_{i20}Bi_{40}$/C	0.323	±	0.033	38.9	±	4.4
$Pd_{60}Ni_{20}Bi_{20}$/C	0.348	±	0.007	65.5	±	7.6
$Pd_{70}Ni_{20}Bi_{10}$/C	0.236	±	0.005	106.3	±	0.5
$Pd_{60}Ni_{40}$/C	0.290	±	0.018	96.0	±	10.4

Even though $Pd_{70}Ni_{20}Bi_{10}$/C exhibits the best results in respect to the onset potential and peak current density (see Table 4-7), the byproduct tolerance is not as good as for $Pd_{60}Ni_{20}Bi_{20}$/C. However, $Pd_{70}Ni_{20}Bi_{10}$/C is the second best catalyst among the tested ones if the total current for the calculation of the byproduct tolerance is used (see Figure 4-12 and Table 4-8). An explanation for this result could be that in the catalyst containing 20% of Bi, more Pd active sites are protected by Bi atoms. However, the reactant is hindered to reach the active sites leading to lower activity and higher stability. In contrast, in the $Pd_{70}Ni_{20}Bi_{10}$/C catalyst only 10% of Bi protects the active sites of Pd from poisoning resulting in a lower byproduct tolerance. However, the active sites are better accessible for ethanol and a higher activity is observed.

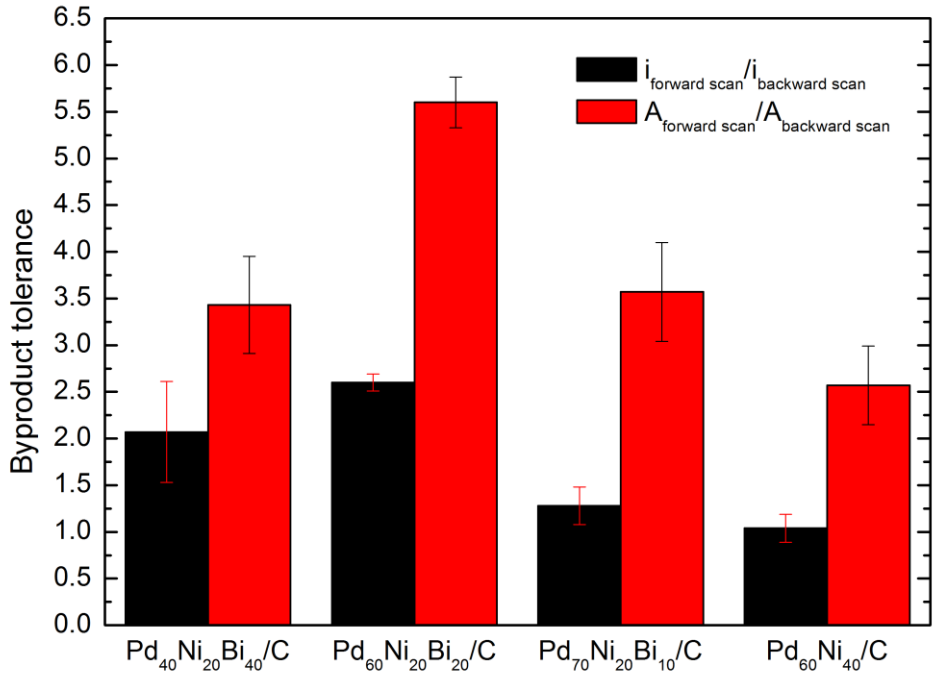

Figure 4-12: Byproduct tolerances of $Pd_{40}Ni_{20}Bi_{40}/C$, $Pd_{60}Ni_{20}Bi_{20}/C$, $Pd_{70}Ni_{20}Bi_{10}/C$ and $Pd_{60}Ni_{40}/C$ catalysts calculated from the peak currents and peak areas, from the CVs recorded in an aqueous solution (1 M KOH and 1 M EtOH) at 30 °C with a scan rate of 10 mV s^{-1}.

Table 4-8: Byproduct tolerances calculated from the peak currents and peak areas of $Pd_{40}Ni_{20}Bi_{40}/C$, $Pd_{60}Ni_{20}Bi_{20}/C$, $Pd_{70}Ni_{20}Bi_{10}/C$ and $Pd_{60}Ni_{40}/C$ catalysts, from the CVs recorded in an aqueous solution (1 M KOH and 1 M EtOH) at 30 °C with a scan rate of 10 mV s^{-1}.

Catalyst	$i_{forward\ scan}/i_{backward\ scan}$		Standard deviation	$A_{forward\ scan}/A_{backward\ scan}$		Standard deviation
$Pd_{40}Ni_{20}Bi_{40}/C$	2.07	±	0.54	3.43	±	0.52
$Pd_{60}Ni_{20}Bi_{20}/C$	2.60	±	0.09	5.60	±	0.27
$Pd_{70}Ni_{20}Bi_{10}/C$	1.28	±	0.20	3.57	±	0.53
$Pd_{60}Ni_{40}/C$	1.04	±	0.15	2.57	±	0.42

4.4.3 Chronoamperometry performance

In the CA measurement (see Figure 4-13), the results correlate with the results obtained from the byproduct tolerance calculations. The $Pd_{60}Ni_{20}Bi_{20}/C$ which exhibited the highest byproduct tolerance was also found to be the most stable one in the CA measurement followed by $Pd_{70}Ni_{20}Bi_{10}/C$ which still had almost 40% of the starting current density after one hour at an applied potential of 0.83 V (see Figure 4-14 and Table 4-9).

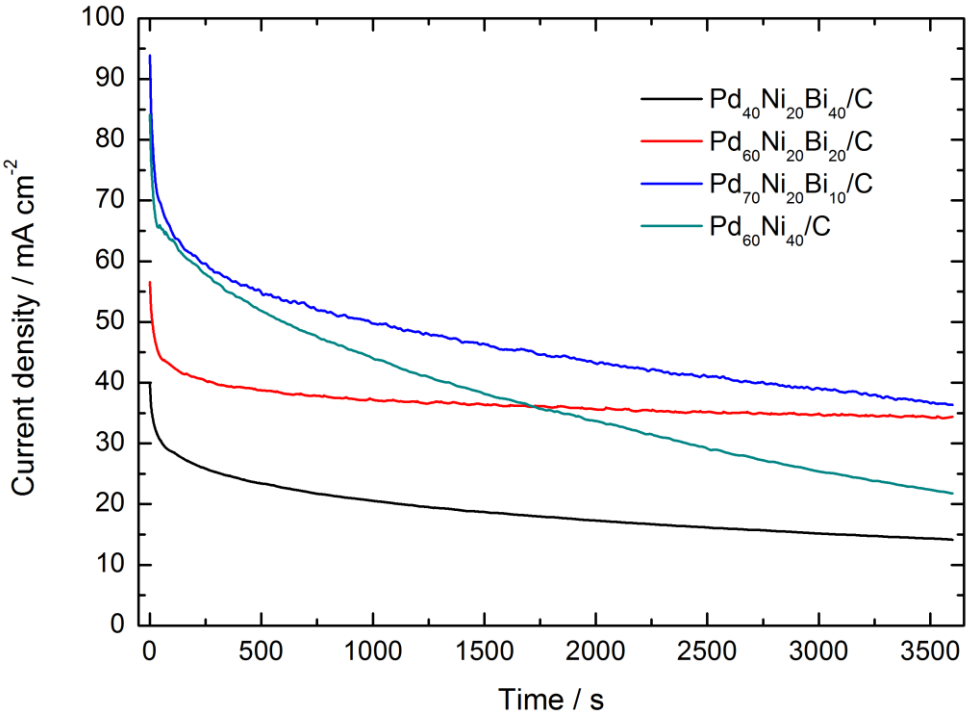

Figure 4-13: CA curves of $Pd_{40}Ni_{20}Bi_{40}/C$, $Pd_{60}Ni_{20}Bi_{20}/C$, $Pd_{70}Ni_{20}Bi_{10}/C$ and $Pd_{60}Ni_{40}/C$ catalysts at 0.83 V vs. RHE in an aqueous solution (1 M KOH and 1 M EtOH) at 30 °C.

Table 4-9: Calculated remaining current densities of $Pd_{40}Ni_{20}Bi_{40}/C$, $Pd_{60}Ni_{20}Bi_{20}/C$, $Pd_{70}Ni_{20}Bi_{10}/C$ and $Pd_{60}Ni_{40}/C$ catalysts after one hour of CA measurement at 0.83 V vs. RHE in an aqueous solution (1 M KOH and 1 M EtOH) at 30 °C.

Catalyst	Remaining current density after 3600 s %		Standard deviation %
$Pd_{40}Ni_{20}Bi_{40}/C$	12.6	±	3.5
$Pd_{60}Ni_{20}Bi_{20}/C$	55.3	±	11.18
$Pd_{70}Ni_{20}Bi_{10}/C$	39.8	±	0.8
$Pd_{60}Ni_{40}/C$	19.4	±	5.6

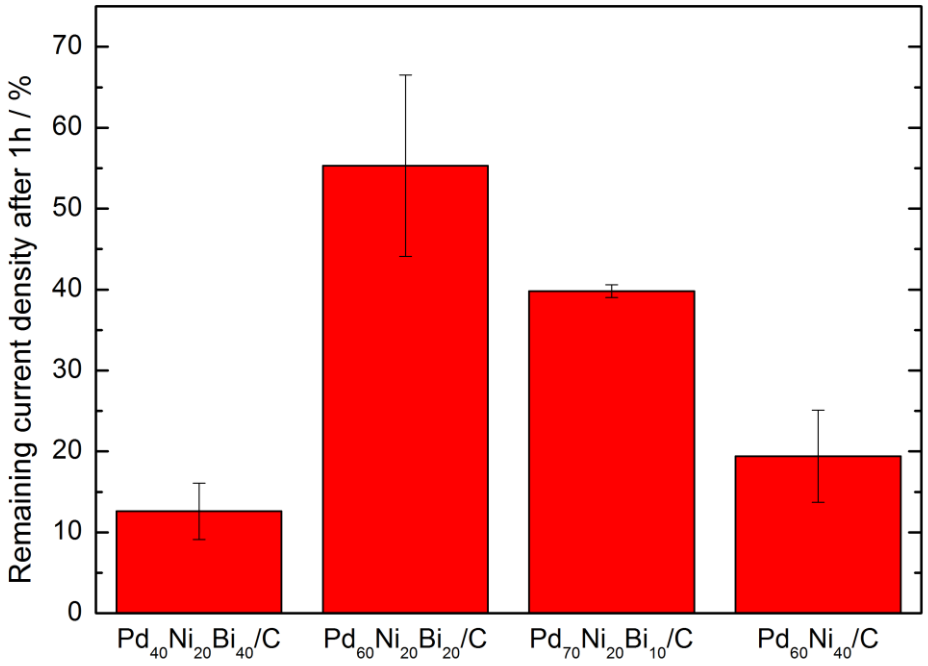

Figure 4-14: Remaining current densities of $Pd_{40}Ni_{20}Bi_{40}/C$, $Pd_{60}Ni_{20}Bi_{20}/C$, $Pd_{70}Ni_{20}Bi_{10}/C$ and $Pd_{60}Ni_{40}/C$ catalysts after one hour of CA measurement at 0.83 V vs. RHE in an aqueous solution (1 M KOH and 1 M EtOH) at 30 °C.

4.5 Further variation of the catalyst composition

Since the previous studies on the influence of Ni and Bi on Pd-based catalysts has shown that a low Bi content enhances the activity of the catalyst, it was attempted to decrease the Bi content even further from 10% to 5%. Additionally, the Pd content was increased to test if the activity would rise further with a higher Pd content. Therefore, the catalysts $Pd_{70}Ni_{25}Bi_5/C$ and $Pd_{80}Ni_{10}Bi_{10}/C$ were synthesized and compared to $Pd_{70}Ni_{20}Bi_{10}/C$ catalyst.

4.5.1 Cyclic voltammetry

The CVs of the $Pd_{70}Ni_{25}Bi_5/C$, $Pd_{80}Ni_{10}Bi_{10}/C$ and $Pd_{70}Ni_{20}Bi_{10}/C$ catalysts exhibit similar curves in 1.0 M KOH alkaline solution (see Figure 4-15). The EASAs of $Pd_{70}Ni_{25}Bi_5/C$ and $Pd_{80}Ni_{10}Bi_{10}/C$ catalysts are lower than the EASA of $Pd_{70}Ni_{20}Bi_{10}/C$ (see Table 4-10 and Figure 4-16).

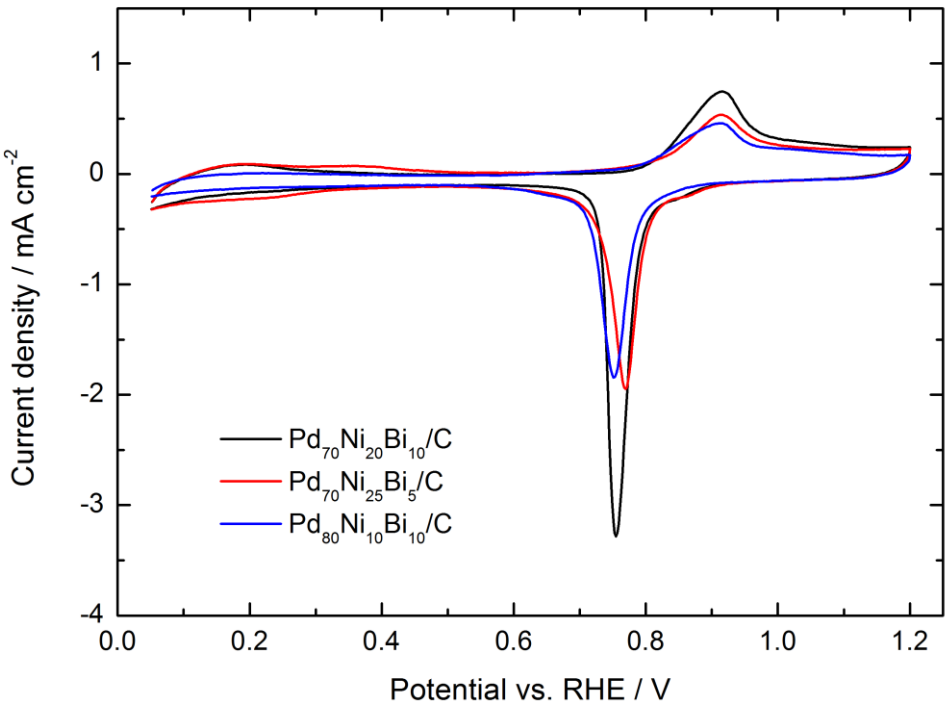

Figure 4-15: CVs of $Pd_{70}Ni_{20}Bi_{10}/C$, $Pd_{70}Ni_{25}Bi_5/C$ and $Pd_{80}Ni_{10}Bi_{10}/C$ catalysts recorded in 1.0 M KOH at 30 °C with a scan rate of 10 mV s^{-1}.

Table 4-10: EASAs of $Pd_{70}Ni_{20}Bi_{10}/C$, $Pd_{70}Ni_{25}Bi_5/C$ and $Pd_{80}Ni_{10}Bi_{10}/C$ catalysts, calculated from CVs recorded in 1.0 M KOH at 30 °C with a scan rate of 10 mV s^{-1}.

Catalyst	EASA mg cm^{-2}		Standard deviation mg cm^{-2}
$Pd_{70}Ni_{20}Bi_{10}/C$	529.7	±	69.0
$Pd_{70}Ni_{25}Bi_5/C$	436.2	±	94.0
$Pd_{80}Ni_{10}Bi_{10}/C$	461.7	±	21.1

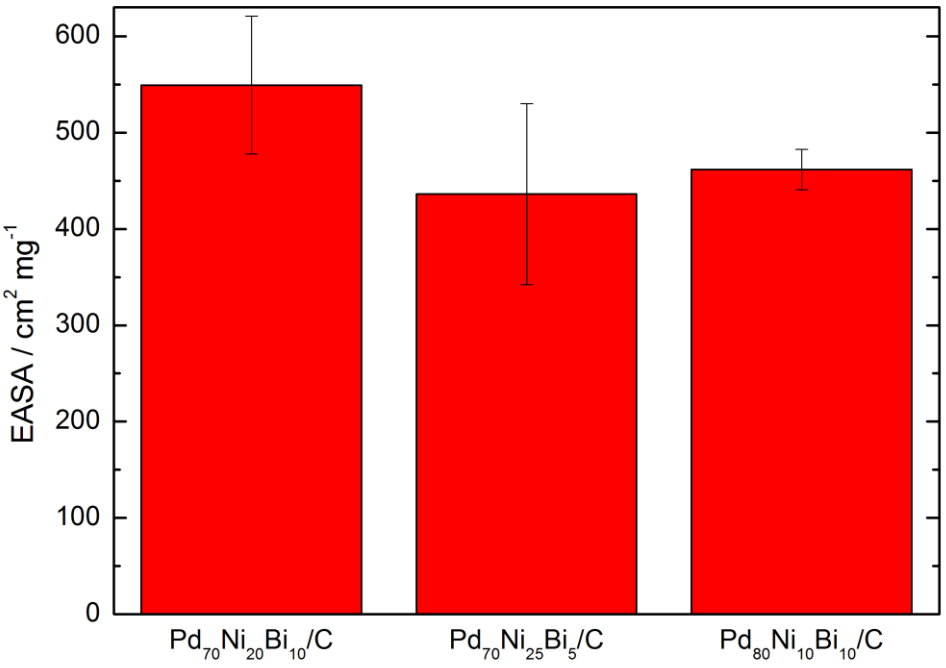

Figure 4-16: EASAs of $Pd_{70}Ni_{20}Bi_{10}/C$, $Pd_{70}Ni_{25}Bi_5/C$ and $Pd_{80}Ni_{10}Bi_{10}/C$ catalysts, calculated from CVs recorded in 1.0 M KOH at 30 °C with a scan rate of 10 mV s^{-1}**.**

4.5.2 Ethanol Oxidation Characteristics

In the EOR measurements, the $Pd_{70}Ni_{25}Bi_5/C$ and $Pd_{80}Ni_{10}Bi_{10}/C$ could not exceed the peak current density of the $Pd_{70}Ni_{20}Bi_{10}/C$ catalyst (see Figure 4-17). However, $Pd_{70}Ni_{25}Bi_5/C$ (0.239 V) has a low onset potential very close to that of $Pd_{70}Ni_{20}Bi_{10}/C$

(0.236 V) (see Table 4-11). This supports the thesis that low amounts of Bi enhance the kinetics at the anode for the EOR in alkaline medium but the increase in peak current density could not be confirmed. In case of the $Pd_{80}Ni_{10}Bi_{10}/C$ catalysts, the onset potential and the peak current density were both reduced compared to $Pd_{70}Ni_{20}Bi_{10}/C$ (see Figure 4-17). This result is also conclusive when taking into account that the Ni content was reduced and the addition of higher amounts of Ni are necessary for a catalyst with high activity [23].

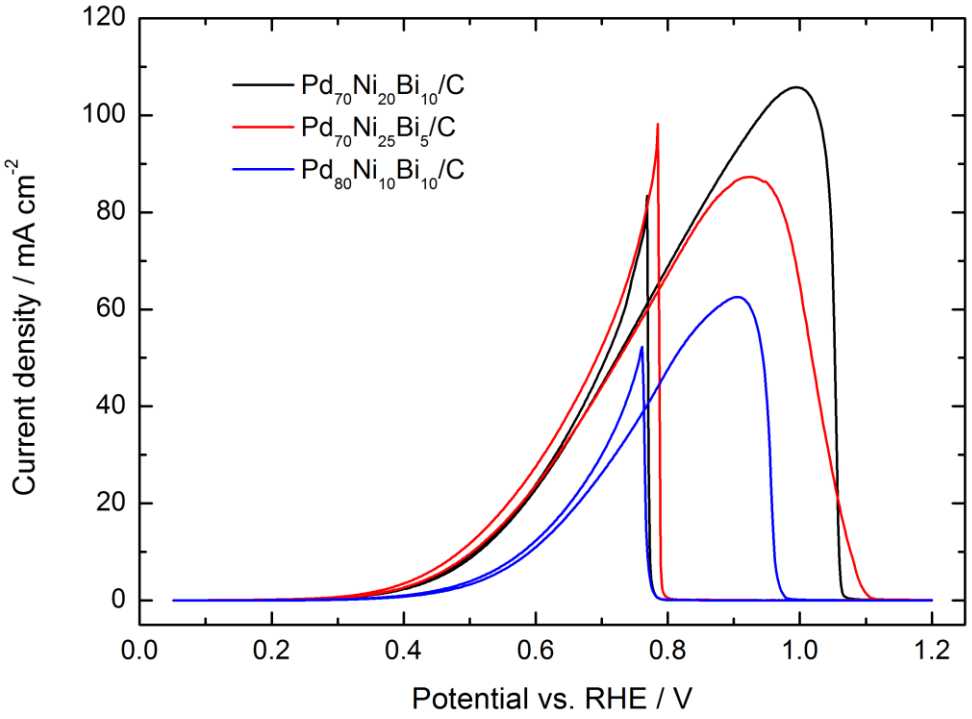

Figure 4-17: CVs of $Pd_{70}Ni_{20}Bi_{10}/C$, $Pd_{70}Ni_{25}Bi_5/C$ and $Pd_{80}Ni_{10}Bi_{10}/C$ catalysts recorded in an aqueous solution (1 M KOH and 1 M EtOH) at 30 °C with a scan rate of 10 mV s^{-1}.

Table 4-11: Onset potentials and peak current densities of $Pd_{70}Ni_{20}Bi_{10}/C$, $Pd_{70}Ni_{25}Bi_5/C$ and $Pd_{80}Ni_{10}Bi_{10}/C$ catalysts, recorded in an aqueous solution (1 M KOH and 1 M EtOH) at 30 °C.

Catalyst	Onset potential V		Standard deviation V	Peak current density mA cm^{-2}		Standard deviation mA cm^{-2}
$Pd_{70}Ni_{20}Bi_{10}/C$	0.236	±	0.005	106.3	±	0.5
$Pd_{70}Ni_{25}Bi_5/C$	0.239	±	0.009	80.8	±	7.2
$Pd_{80}Ni_{10}Bi_{10}/C$	0.274	±	0.008	63.8	±	6.6

As expected, the byproduct tolerance of $Pd_{70}Ni_{25}Bi_5/C$ decreases when the Bi content is reduced from 10 to 5%. Also for the $Pd_{80}Ni_{10}Bi_{10}/C$ catalyst the byproduct tolerance is reduced compared to $Pd_{70}Ni_{20}Bi_{10}/C$ but still higher than for $Pd_{70}Ni_{25}Bi_5/C$ (see Figure 4-18 and Table 4-12).

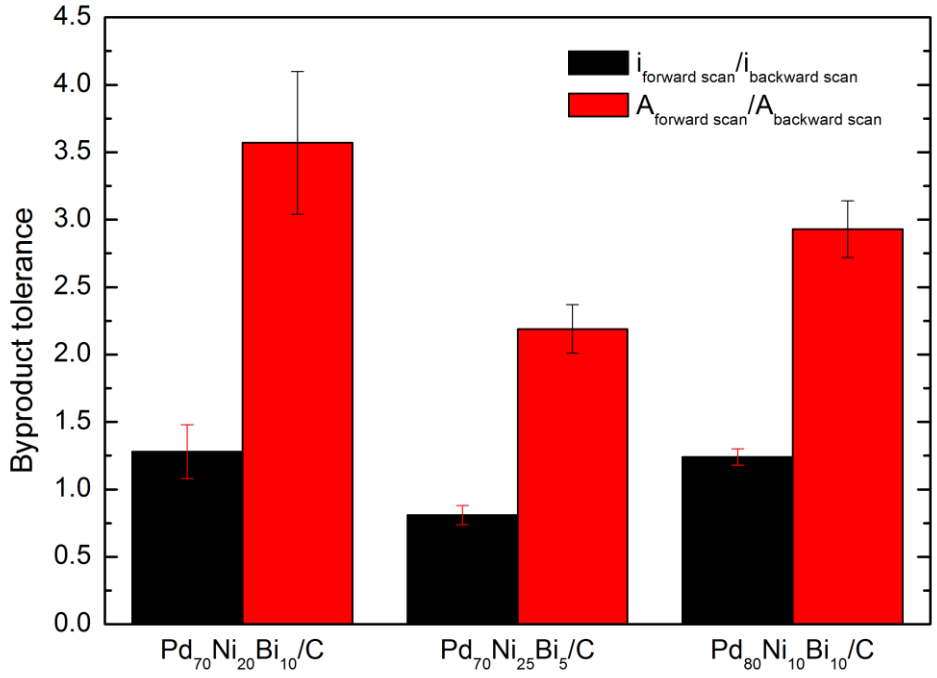

Figure 4-18: Byproduct tolerances of $Pd_{70}Ni_{20}Bi_{10}/C$, $Pd_{70}Ni_{25}Bi_5/C$ and $Pd_{80}Ni_{10}Bi_{10}/C$ catalysts, calculated from the peak currents and peak areas, from the CVs recorded in an aqueous solution (1 M KOH and 1 M EtOH) at 30 °C with a scan rate of 10 mV s^{-1}.

Table 4-12: Byproduct tolerances calculated from the peak current densities and peak areas of $Pd_{70}Ni_{20}Bi_{10}/C$, $Pd_{70}Ni_{25}Bi_5/C$ and $Pd_{80}Ni_{10}Bi_{10}/C$ catalysts, from the CVs recorded in an aqueous solution (1 M KOH and 1 M EtOH) at 30 °C with a scan rate of 10 mV s^{-1}.

Catalyst	$i_{forward\ scan}/i_{backward\ scan}$		Standard deviation	$A_{forward\ scan}/A_{backward\ scan}$		Standard deviation
$Pd_{70}Ni_{20}Bi_{10}/C$	1.28	±	0.20	3.57	±	0.53
$Pd_{70}Ni_{25}Bi_5/C$	0.81	±	0.07	2.19	±	0.18
$Pd_{80}Ni_{10}Bi_{10}/C$	1.24	±	0.06	2.93	±	0.21

4.5.3 Chronoamperometry performance

In the CA measurements, the $Pd_{70}Ni_{25}Bi_5/C$ and $Pd_{80}Ni_{10}Bi_{10}/C$ catalysts also show lower stability than $Pd_{70}Ni_{20}Bi_{10}/C$ (see Figure 4-19, Figure 4-20 and Table 4-13). However, the results are still better than for Pd/C and $Pd_{60}Ni_{40}/C$ showing the positive effect of Bi on the stability.

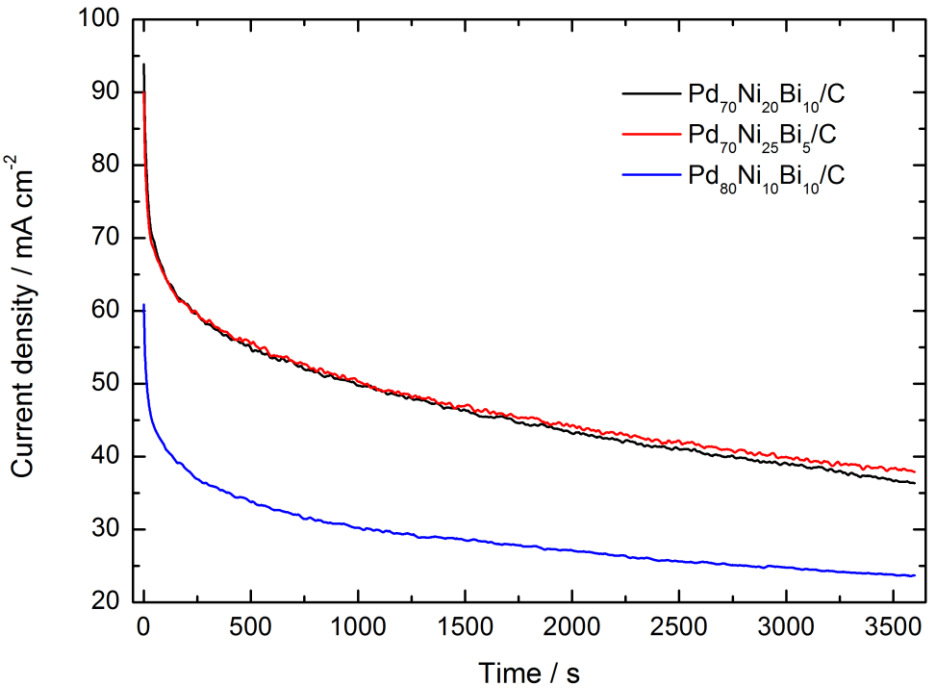

Figure 4-19: CA curves of $Pd_{70}Ni_{20}Bi_{10}/C$, $Pd_{70}Ni_{25}Bi_5/C$ and $Pd_{80}Ni_{10}Bi_{10}/C$ catalysts at 0.83 V vs. RHE in an aqueous solution (1 M KOH and 1 M EtOH) at 30 °C.

Table 4-13: Calculated remaining current densities of $Pd_{70}Ni_{20}Bi_{10}/C$, $Pd_{70}Ni_{25}Bi_5/C$ and $Pd_{80}Ni_{10}Bi_{10}/C$ catalysts after one hour of CA measurement at 0.83 V vs. RHE in an aqueous solution (1 M KOH and 1 M EtOH) at 30 °C.

Catalyst	Remaining current density after 3600 s %		Standard deviation %
$Pd_{70}Ni_{20}Bi_{10}/C$	39.8	±	0.8
$Pd_{70}Ni_{25}Bi_5/C$	33.8	±	2.7
$Pd_{80}Ni_{10}Bi_{10}/C$	32.9	±	7.7

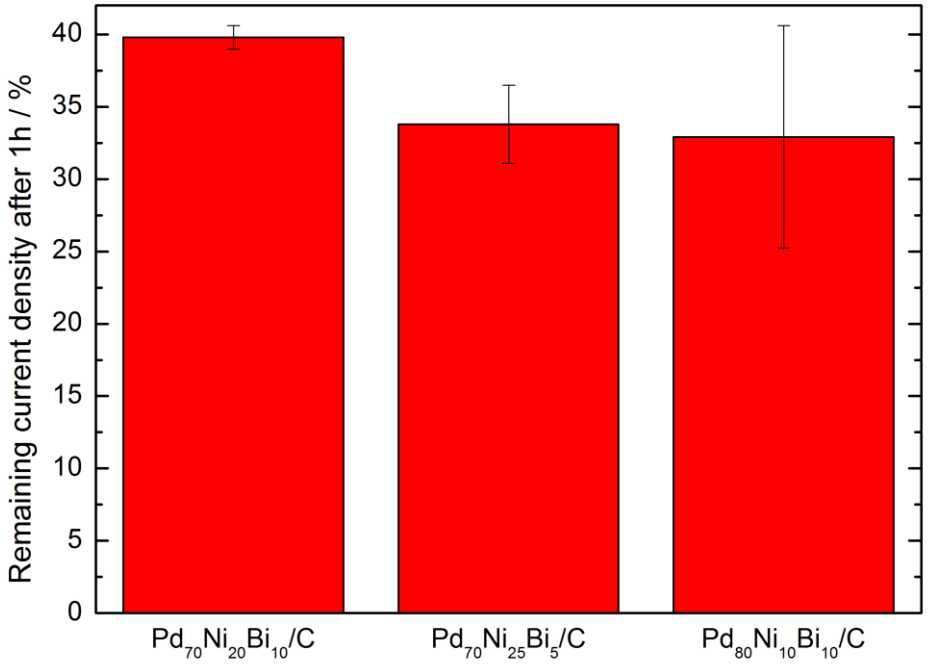

Figure 4-20: Remaining current densities of $Pd_{70}Ni_{20}Bi_{10}/C$, $Pd_{70}Ni_{25}Bi_5/C$ and $Pd_{80}Ni_{10}Bi_{10}/C$ catalysts after one hour of CA measurement at 0.83 V vs. RHE in an aqueous solution (1 M KOH and 1 M EtOH) at 30 °C.

4.6 Summary *ex-situ* measurements

It can be concluded that higher amounts of Ni in Pd-based anode catalysts for the alkaline DEFC enhance the activity for the EOR. In case of Bi, it is confirmed that lower amounts of Bi enhance the activity and kinetics at the anode for the EOR in alkaline medium. This was observed as a low onset potential and high peak current density for catalysts with low Bi concentration. It was also found that a higher concentration of Bi (20%) improves the byproduct tolerance and the stability of the catalyst.

The $Pd_{70}Ni_{20}Bi_{10}/C$ catalyst was found the most active catalyst among all tested catalysts (see Figure 4-21) and exhibited the second best results in terms of byproduct tolerance. The $Pd_{60}Ni_{20}Bi_{20}/C$ shows the best byproduct tolerance and stability which are also very important features for the application of a catalyst in a single cell (see Figure 4-22). Due to the good results, those catalysts were investigated in a single cell measurement.

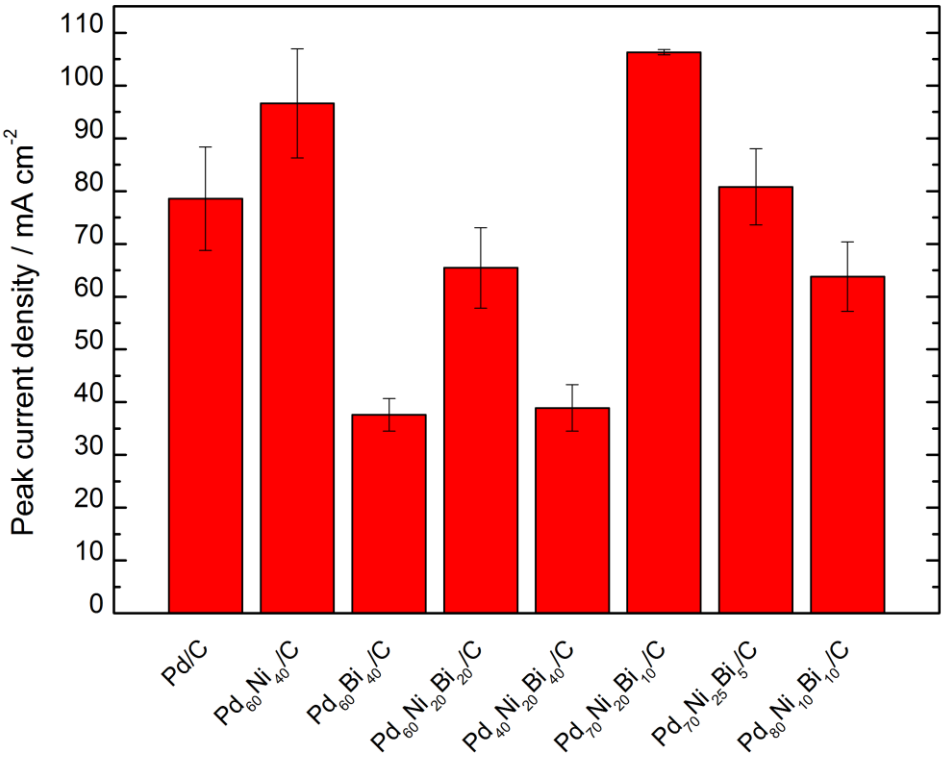

Figure 4-21: Peak current densities of all tested catalysts that were reached in the CV measurements recorded in an aqueous solution (1 M KOH and 1 M EtOH) at 30 °C with a scan rate of 10 mV s^{-1}.

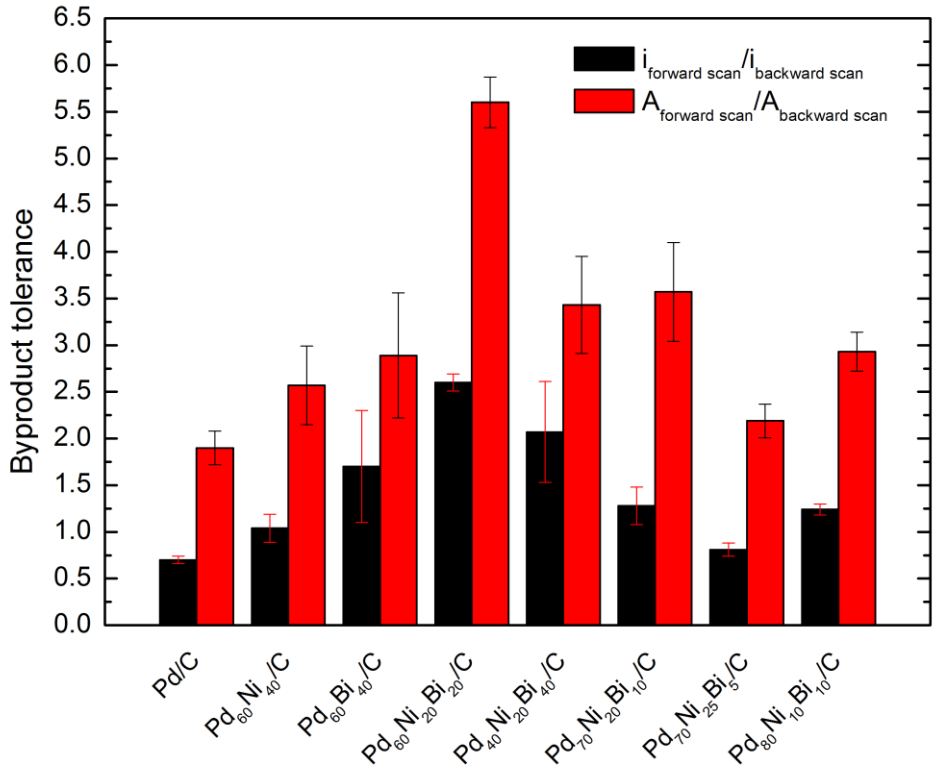

Figure 4-22: Byproduct stabilities of all catalysts calculated from the peak currents and the peak areas, from the CVs recorded in an aqueous solution (1 M KOH and 1 M EtOH) at 30 °C with a scan rate of 10 mV s^{-1}.

4.7 *In-situ* characterization

The $Pd_{60}Ni_{20}Bi_{20}/C$ and $Pd_{70}Ni_{20}Bi_{10}/C$ catalysts were tested in a single cell and compared to the Pd/C as reference. The perovskite cathode catalyst $(La_{0.8}Sr_{0.2})_{0.95}MnO_{3-x}$ and 6.0 M KOH as electrolyte were used. The fuel an aqueous solution containing 6.0 M KOH and 1.0 M EtOH, was provided with a flow rate of 10 mL min^{-1} at the anode. Oxygen was provided with a flow rate of approximately 20 mL min^{-1} at the cathode. The U-I polarization curves of single cell measurements were recorded and their power densities were calculated. Additionally, the anode potential was recorded, using a Luggin capillary, during the cell measurement. For the single cell tests with the anodes Pd/C and $Pd_{60}Ni_{20}Bi_{20}/C$, the same cathode was used. The measurement with the Pd/C anode was performed first. For the measurement of $Pd_{70}Ni_{20}Bi_{10}/C$ a new cathode was fabricated.

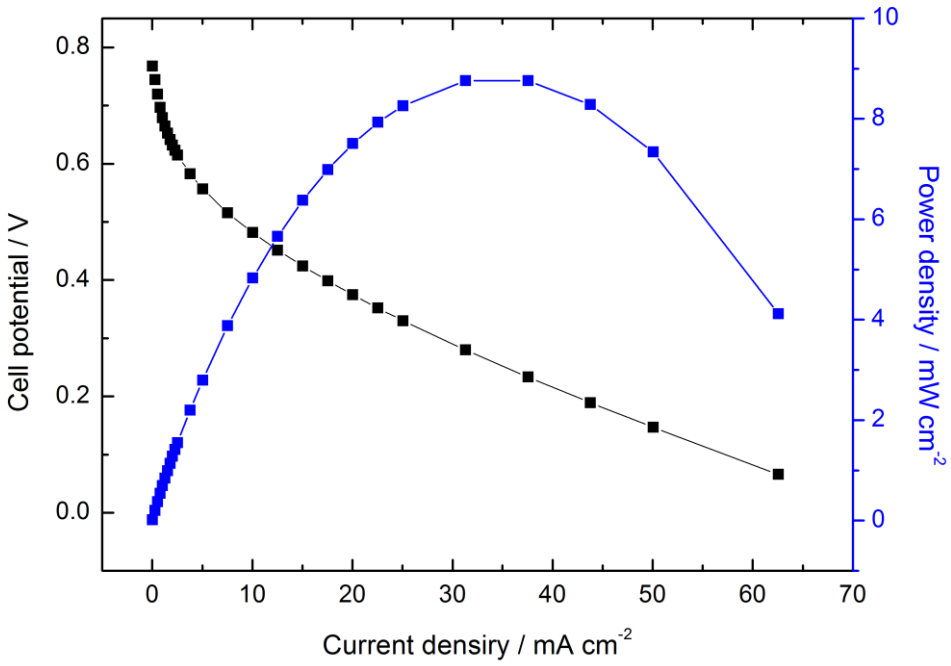

Figure 4-23: U-I curve and power density curve of a single cell at 30 °C using Pd/C as anode catalyst (1 mg_{Pd} cm^{-2}), $(La_{0.8}Sr_{0.2})_{0.95}MnO_{3-x}$ as cathode catalyst and 6.0 M KOH as electrolyte. Fuel at anode: aqueous solution (6.0 M KOH and 1.0 M EtOH) with 10 mL min^{-1}, fuel at the cathode: O_2 with 20 mL min^{-1}.

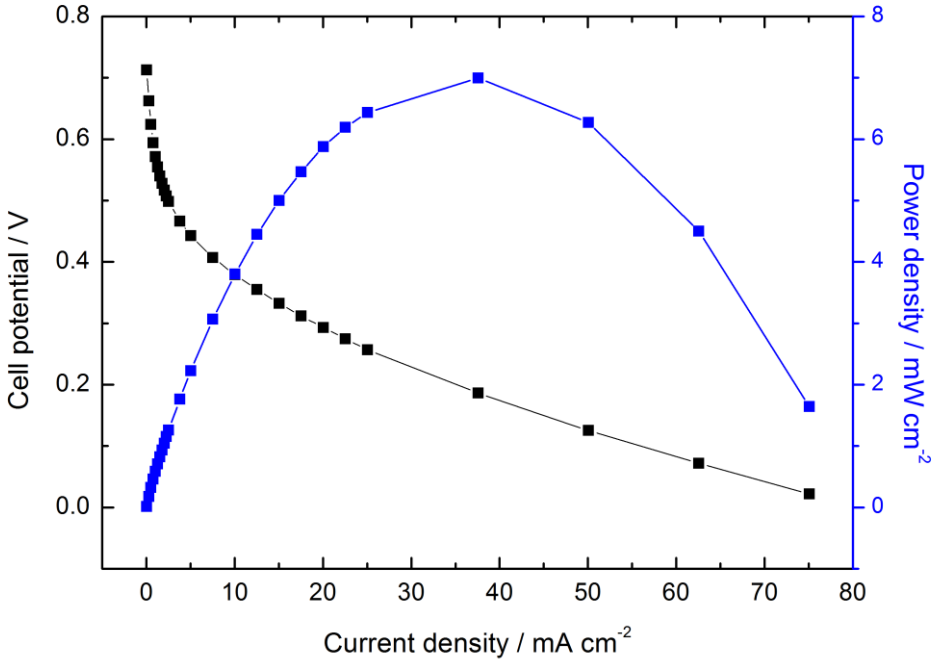

Figure 4-24: U-I curve and power density of a single cell at 30 °C using $Pd_{60}Ni_{20}Bi_{20}/C$ as anode catalyst (1 mg_{Pd} cm^{-2}), $(La_{0.8}Sr_{0.2})_{0.95}MnO_{3-x}$ as cathode catalyst and 6.0 M KOH as electrolyte. Fuel at anode: aqueous solution (6.0 M KOH and 1.0 M EtOH) with 10 mL min^{-1}, fuel at the cathode: O_2 with 20 mL min^{-1}.

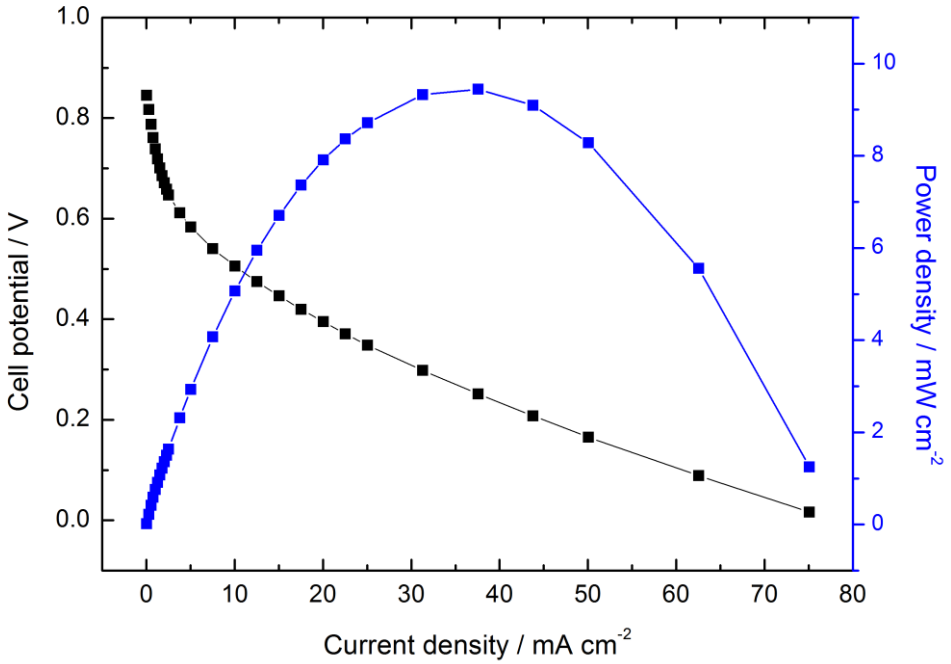

Figure 4-25: U-I curve and power density of a single cell at 30 °C using $Pd_{70}Ni_{20}Bi_{10}/C$ as anode catalyst (1 mg_{Pd} cm^{-2}), $(La_{0.8}Sr_{0.2})_{0.95}MnO_{3-x}$ as cathode catalyst and 6 M KOH as electrolyte. Fuel at anode: aqueous solution (6.0 M KOH and 1.0 M EtOH) with 10 mL min^{-1}, fuel at the cathode: O_2 with 20 mL min^{-1}.

From the polarization curves of the cell measurements with Pd/C, $Pd_{60}Ni_{20}Bi_{20}$/C and $Pd_{70}Ni_{20}Bi_{10}$/C anodes, it is observed that the open circuit voltage (OCV) can be drastically increased in case of $Pd_{70}Ni_{20}Bi_{10}$/C compared to Pd/C (see Figure 4-23, Figure 4-24 and Figure 4-25). The OCV using the $Pd_{70}Ni_{20}Bi_{10}$/C anode is 79 mV higher than in the single cell measurement with the Pd/C anode and even 126 mV higher than for cell measurement with the $Pd_{60}Ni_{20}Bi_{20}$/C anode (see Table 4-14). Those results are in accordance with the results of the *ex-situ* measurements. In *ex-situ* measurements, the onset potentials also increased in the same order $Pd_{70}Ni_{20}Bi_{10}$/C < Pd/C < $Pd_{60}Ni_{20}Bi_{20}$/C as the OCV and the anode open circuit potential (OCP) in the single cell measurements (see Figure 4-27 and Table 4-15). The same correlation is found for the maximum power density; the highest power density is also found for $Pd_{70}Ni_{20}Bi_{10}$/C which also showed the highest peak current density in the *ex-situ* EOR measurement (see Table 4-14 and Figure 4-26).

Table 4-14: Obtained OCVs and calculated power densities of single cell measurements with Pd/C, $Pd_{60}Ni_{20}Bi_{20}$/C and $Pd_{70}Ni_{20}Bi_{10}$ anode catalysts.

Anode catalyst	Open circuit voltage (OCV) V	Maximum power density mW cm^{-2}
Pd/C	0.770	8.76
$Pd_{60}Ni_{20}Bi_{20}$/C	0.723	6.99
$Pd_{70}Ni_{20}Bi_{10}$/C	0.849	9.44

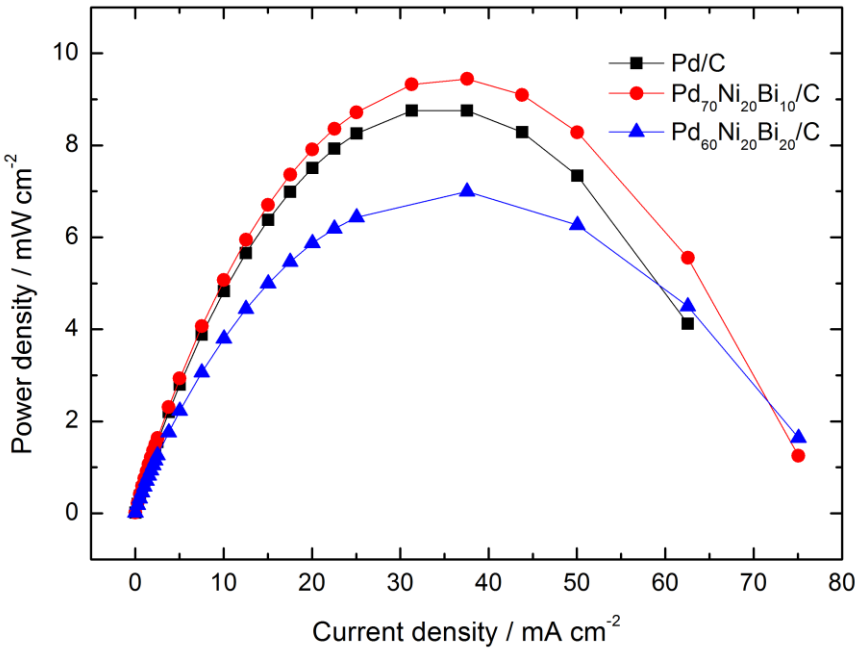

Figure 4-26: Power density curves of the single cells at 30 °C using Pd/C, $Pd_{60}Ni_{20}Bi_{20}$/C and $Pd_{70}Ni_{20}Bi_{10}$/C as anode catalysts (1 mg_{Pd} cm^{-2}), $(La_{0.8}Sr_{0.2})_{0.95}MnO_{3-x}$ as cathode catalyst and 6.0 M KOH as electrolyte. Fuel at anode: aqueous solution (6.0 M KOH and 1.0 M EtOH) with 10 mL min^{-1}, fuel at the cathode: O_2 with 20 mL min^{-1}.

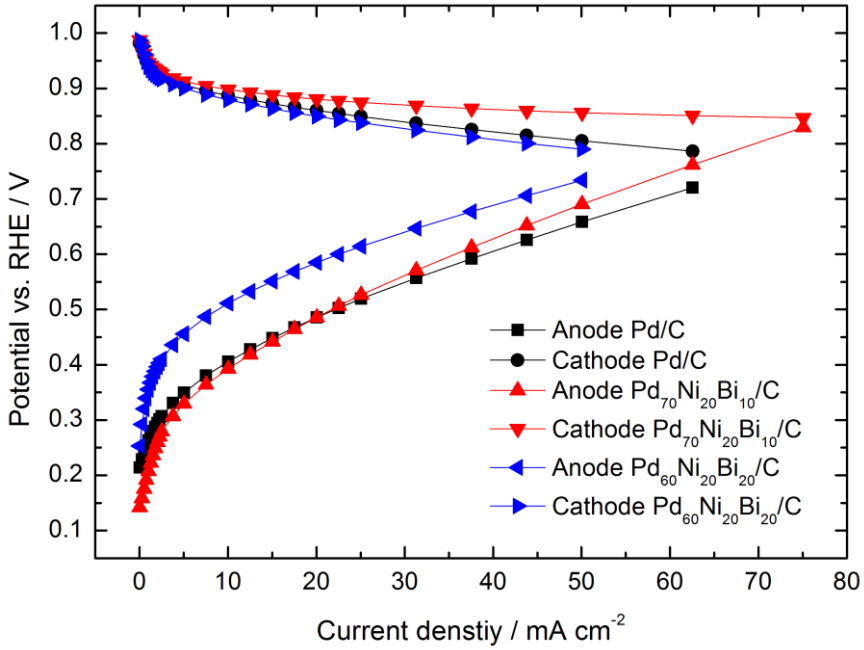

Figure 4-27: Half-cell performances of single cells at 30 °C using Pd/C, $Pd_{60}Ni_{20}Bi_{20}$/C and $Pd_{70}Ni_{20}Bi_{10}$/C as anode catalysts (1 mg_{Pd} cm^{-2}), $(La_{0.8}Sr_{0.2})_{0.95}MnO_{3-x}$ as cathode catalyst and 6 M KOH as electrolyte. Fuel at anode: aqueous solution (6.0 M KOH and 1.0 M EtOH) with 10 mL min^{-1}, fuel at the cathode: O_2 with 20 mL min^{-1}.

Table 4-15: OCV of single cell measurements carried out at 30 °C, measured anode OCP of Pd/C, $Pd_{60}Ni_{20}Bi_{20}$/C and $Pd_{70}Ni_{20}Bi_{10}$/C and calculated corresponding cathode OCP. Fuel at anode: aqueous solution (6.0 M KOH and 1.0 M EtOH) with 10 mL min^{-1}, fuel at the cathode: O_2 with 20 mL min^{-1}.

Anode catalyst	OCV V	Anode OCP V	Cathode OCP(calculated) V
Pd/C	0.770	0.212	0.982
$Pd_{60}Ni_{20}Bi_{20}$/C	0.723	0.231	0.954
$Pd_{70}Ni_{20}Bi_{10}$/C	0.849	0.139	0.988

For cell measurements with the anodes Pd/C and $Pd_{60}Ni_{20}Bi_{20}$/C, the same cathode was used. The measurement using the Pd/C anode was performed first. A slight potential decrease of the cathode in the second cell measurement with the $Pd_{60}Ni_{20}Bi_{20}$/C anode is observed indicating an occurring degradation process (Figure 4-27). In the comparison of the half-cell performances it is also observed that not only the different anodes, but also the cathodes exhibit different potential curves. Even though the cathodes have the same composition, the electrode fabrication process is rather complicated and the resulting cathodes can vary in their performances.

The measured anode potentials show that the OCP of $Pd_{70}Ni_{20}Bi_{10}$/C is far below the one of Pd/C and $Pd_{60}Ni_{20}Bi_{20}$/C (see Table 4-15). This proofs that small amounts of Bi enhance the EOR kinetics. It is difficult to compare the obtained maximum power densities and OCVs to literature as the single cell composition and the test parameters are different in most cases. Mainly, anion exchange membranes and Pt-based catalyst are used for DEFC single cell measurements [44,15].

5 Conclusion and Outlook

In this master's thesis the influence of Ni and Bi on Pd-based anode catalysts for the alkaline direct ethanol fuel cell was investigated. Novel ternary catalysts containing Pd, Ni and Bi were synthesized using the simultaneous reduction method. It was attempted to combine enhanced activity, good byproduct tolerance and stability. Therefore, the atomic ratios of those metals were varied to find a catalyst with high activity and stability.

The addition of a relatively high amount of Ni (~40wt.%) to Pd led to a significant increase in peak current density of 22%. The addition of Bi (~40wt.%) to Pd resulted in a very good byproduct tolerance of the catalyst. In the attempt to combine the enhanced activity and the excellent byproduct tolerance, ternary PdNiBi/C catalysts were prepared, whereby the $Pd_{60}Ni_{20}Bi_{20}$/C catalyst exhibited the best byproduct tolerance and stability. The $Pd_{70}Ni_{20}Bi_{10}$/C catalyst outperformed all other tested catalysts, in terms of activity for the EOR. The onset potential was 54 mV lower and the peak current density was more than 10 mA cm^{-2} higher compared to the $Pd_{60}Ni_{40}$/C catalyst, which was found the second most active catalyst. Furthermore, the $Pd_{70}Ni_{20}Bi_{10}$/C catalyst exhibited the second best results in terms of byproduct tolerance and stability after the $Pd_{60}Ni_{20}Bi_{20}$/C catalyst.

The excellent results from the *ex-situ* tests of the $Pd_{70}Ni_{20}Bi_{10}$/C and $Pd_{60}Ni_{20}Bi_{20}$/C catalysts were confirmed in a single cell measurement. The power density of the $Pd_{70}Ni_{20}Bi_{10}$/C exceeded the power density of the Pd/C catalyst by ~8% serving as benchmark. In particular, the low onset potential of the $Pd_{70}Ni_{20}Bi_{10}$/C catalyst is remarkable.

Further experiments focus on variations in the synthesis method for the catalysts which allow a more controlled deposition of the metal particles on the support and defined particle sizes. Additionally, single cell measurements using higher loadings of $Pd_{70}Ni_{20}Bi_{10}$/C as anode catalyst in the alkaline DEFC are investigated. The effects of increased temperature, fuel composition and fuel flow rate are also of interest for upcoming research activities.

6 References

[1] U.S. Energy Information Administration "International Energy Outlook 2016, Chapter 1: World energy demand and economic outlook," pp. 7–17, 2016.

[2] H. Chen, T. N. Cong, W. Yang, C. Tan, Y. Li, and Y. Ding, “Progress in electrical energy storage system: A critical review,” *Prog. Nat. Sci.*, vol. 19, no. 3, pp. 291–312, 2009.

[3] E-Control Stromkennzeichnungsbericht 2015, “Informiert sein. - Wo immer man bei Strom Gewissheit möchte,” 2015.

[4] U.S. Energy Information Administration "Net Generation by Energy Source: All Sectors 2005-2015", Retrieved from: https://www.eia.gov/electricity/annual/html/epa_03_01_a.html (19/10/2017)

[5] S. Y. Tee, K. Y. Win, W. S. Teo *et al.*, “Recent Progress in Energy-Driven Water Splitting,” *Adv. Sci.*, vol. 4, no. 5, pp. 1-24, 2017.

[6] L. An, T. S. Zhao, and Y. S. Li, “Carbon-neutral sustainable energy technology: Direct ethanol fuel cells,” *Renew. Sustain. Energy Rev.*, vol. 50, pp. 1462–1468, 2015.

[7] R. Muktham, S. K. Bhargava, S. Bankupalli, and A. S. Ball, “A Review on 1st and 2nd Generation Bioethanol Production-Recent Progress,” *J. Sustain. Bioenergy Syst.*, vol. 6, no. 3, pp. 72–92, 2016.

[8] A. Kirubakaran, S. Jain, and R. K. Nema, “A review on fuel cell technologies and power electronic interface,” *Renew. Sustain. Energy Rev.,* vol. 13, pp. 2430–2440, 2009.

[9] R. Dillon, S. Srinivasan, A. S. Aricò, and V. Antonucci, “International activities in DMFC R&D: Status of technologies and potential applications,” *J. Power*

Sources, vol. 127, no. 1–2, pp. 112–126, 2004.

[10] C. Bianchini and P. K. Shen, “Palladium-Based Electrocatalysts for Alcohol Oxidation in Half Cells and in Direct Alcohol Fuel Cells,” *Chem. Rev.*, vol. 108, no. 9, pp. 4183–4206, 2009.

[11] E. H. Yu, U. Krewer, and K. Scott, “Principles and materials aspects of direct alkaline alcohol fuel cells,” *Energies*, vol. 3, no. 8, pp. 1499–1528, 2010.

[12] M. L. Perry and T. F. Fuller, “A Historical Perspective of Fuel Cell Technology in the 20th Century,” *J. Electrochem. Soc.*, vol. 149, no. 7, pp. 59-67, 2002.

[13] E. I. Ortiz-Rivera, A. L. Reyes-Hernandez and R. A. Febo, “Understanding the History of Fuel Cells,” *Electr. Power*, vol. 2, pp. 117–122, 2007.

[14] O. Z. Sharaf, “An overview of fuel cell technology : Fundamentals and applications,” *Renew. Sustain. Energy Rev.*, vol. 32, pp. 810–853, 2014.

[15] M. Z. F. Kamarudin, S. K. Kamarudin, M. S. Masdar, and W. R. W. Daud, “Review: Direct ethanol fuel cells,” *Int. J. Hydrogen Energy*, vol. 38, no. 22, pp. 9438–9453, 2013.

[16] L. An, T. S. Zhao, Q. X. Wu, and L. Zeng, “Comparison of different types of membrane in alkaline direct ethanol fuel cells,” *Int. J. Hydrogen Energy*, vol. 37, no. 19, pp. 14536–14542, 2012.

[17] J. R. Varcoe, R. C. T. Slade, E. Lam How Yee, S. D. Poynton, D. J. Driscoll, and D. C. Apperley, “Poly(ethylene-co-tetrafluoroethylene)-derived radiation-grafted anion-exchange membrane with properties specifically tailored for application in metal-cation-free alkaline polymer electrolyte fuel cells,” *Chem. Mater.*, vol. 19, no. 10, pp. 2686–2693, 2007.

[18] Y. Xiong, J. Fang, Q. H. Zeng, and Q. L. Liu, “Preparation and characterization of cross-linked quaternized poly(vinyl alcohol) membranes for anion exchange

membrane fuel cells," *J. Memb. Sci.*, vol. 311, no. 1–2, pp. 319–325, 2008.

[19] H. Hou, G. Sun, R. He, Z. Wu, and B. Sun, "Alkali doped polybenzimidazole membrane for high performance alkaline direct ethanol fuel cell," vol. 182, pp. 95–99, 2008.

[20] Q. Tang, L. Jiang, J. Qi, Q. Jiang, S. Wang, and G. Sun, "One step synthesis of carbon-supported Ag/MnyOx composites for oxygen reduction reaction in alkaline media," *Appl. Catal. B Environ.*, vol. 104, no. 3–4, pp. 337–345, 2011.

[21] I. Grimmer, P. Zorn, S. Weinberger *et al.*, "Ethanol tolerant precious metal free cathode catalyst for alkaline direct ethanol fuel cells," *Electrochim. Acta*, vol. 228, pp. 325–331, 2017.

[22] C. Xu, L. Cheng, P. Shen, and Y. Liu, "Methanol and ethanol electrooxidation on Pt and Pd supported on carbon microspheres in alkaline media," *Electrochem. commun.*, vol. 9, no. 5, pp. 997–1001, 2007.

[23] Z. Zhang, L. Xin, K. Sun, and W. Li, "Pd-Ni electrocatalysts for efficient ethanol oxidation reaction in alkaline electrolyte," *Int. J. Hydrogen Energy*, vol. 36, no. 20, pp. 12686–12697, 2011.

[24] Z. X. Liang, T. S. Zhao, J. B. Xu, and L. D. Zhu, "Mechanism study of the ethanol oxidation reaction on palladium in alkaline media," *Electrochim. Acta*, vol. 54, no. 8, pp. 2203–2208, 2009.

[25] P. K. Shen and C. Xu, "Alcohol oxidation on nanocrystalline oxide Pd/C promoted electrocatalysts," *Electrochem. commun.*, vol. 8, no. 1, pp. 184–188, 2006.

[26] S. Y. Shen, T. S. Zhao, J. B. Xu, and Y. S. Li, "Synthesis of PdNi catalysts for the oxidation of ethanol in alkaline direct ethanol fuel cells," vol. 195, pp. 1001–1006, 2010.

[27] A. O. Neto, M. M. Tusi, N. S. De Oliveira Polanco, S. G. Da Silva, M. Coelho Dos Santos, and E. V. Spinacé, “PdBi/C electrocatalysts for ethanol electro-oxidation in alkaline medium,” *Int. J. Hydrogen Energy*, vol. 36, no. 17, pp. 10522–10526, 2011.

[28] R. Jiang, D. T. Tran, J. P. McClure, and D. Chu, “A Class of (Pd−Ni−P) Electrocatalysts for the Ethanol Oxidation Reaction in Alkaline Media,” *ACS Catal.*, vol. 4, pp. 2577-2586, 2014.

[29] C. Bianchini, V. Bambagioni, J. Filippi *et al.*, “Selective oxidation of ethanol to acetic acid in highly efficient polymer electrolyte membrane-direct ethanol fuel cells,” *Electrochem. commun.*, vol. 11, no. 5, pp. 1077–1080, 2009.

[30] C. Lamy, C. Coutanceau, and J. M. Leger, *The Direct Ethanol Fuel Cell: A Challenge to Convert Bioethanol Cleanly into Electric Energy*. pp. 1-46, 2009.

[31] C. Lamy, E. M. Belgsir, and J. M. Léger, “Electrocatalytic oxidation of aliphatic alcohols: Application to the direct alcohol fuel cell (DAFC),” *J. Appl. Electrochem.*, vol. 31, no. 7, pp. 799–809, 2001.

[32] N. Hoshi, M. Nakamura, N. Maki, S. Yamaguchi, and A. Kitajima, “Structural effects on voltammograms of the low index planes of palladium and Pd(S)-[n(1 0 0)×(1 1 1)] surfaces in alkaline solution,” *J. Electroanal. Chem.*, vol. 624, no. 1–2, pp. 134–138, 2008.

[33] B. Geboes, I. Mintsouli, B. Wouters *et al.*, “Applied Catalysis B : Environmental Surface and electrochemical characterisation of a Pt-Cu/C nano-structured electrocatalyst , prepared by galvanic displacement,” *Applied Catal. B, Environ.*, vol. 150–151, pp. 249–256, 2014.

[34] R. Pattabiraman, “Electrochemical investigations on carbon supported palladium catalysts,” *Appl. Catal. A Gen.*, vol. 153, pp. 9–20, 1997.

[35] Y. Qin, H. Yang, X. Zhang *et al.*, “Electrophoretic deposition of network-like

carbon nanofibers as a palladium catalyst support for ethanol oxidation in alkaline media," *Carbon*, vol. 48, no. 12, pp. 3323–3329, 2010.

[36] Y. W. Lee, S. B. Han, and K. W. Park, "Electrochemical properties of Pd nanostructures in alkaline solution," *Electrochem. commun.*, vol. 11, no. 10, pp. 1968–1971, 2009.

[37] R. C. Sekol, M. Carmo, G. Kumar *et al.*, "Pd-Ni-Cu-P metallic glass nanowires for methanol and ethanol oxidation in alkaline media," *Int. J. Hydrogen Energy*, vol. 38, no. 26, pp. 11248–11255, 2013.

[38] W. Winkler and P. Nehter, *Thermodynamics of Fuel Cells*, pp. 13–50, 2008.

[39] C. Grimmer, R. Zacharias, M. Grandi *et al.*, "Carbon Supported Ruthenium as Anode Catalyst for Alkaline Direct Borohydride Fuel Cells," *J. Phys. Chem.*, vol. 119, pp. 23839–23844, 2015.

[40] K. Shinozaki, J. W. Zack, R. M. Richards, B. S. Pivovar, and S. S. Kocha, "Oxygen Reduction Reaction Measurements on Platinum Electrocatalysts Utilizing Rotating Disk Electrode Technique: I. Impact of Impurities, Measurement Protocols and Applied Corrections," *J. Electrochem. Soc.*, vol. 162, no. 10, pp. F1144–F1158, 2015.

[41] B. G. Pollet and J. T. E. Goh, "The importance of ultrasonic parameters in the preparation of fuel cell catalyst inks," *Electrochim. Acta*, vol. 128, pp. 292–303, 2014.

[42] V. R. Radmilovi, "Applied Catalysis B : Environmental Electrochemical oxidation of ethanol on palladium-nickel nanocatalyst in alkaline media," *Applied Catal. B, Environ.*, vol. 189, pp. 110–118, 2016.

[43] M. Simões, S. Baranton, and C. Coutanceau, "Influence of bismuth on the structure and activity of Pt and Pd nanocatalysts for the direct electrooxidation of NaBH4," *Electrochim. Acta*, vol. 56, no. 1, pp. 580–591, 2010.

[44] I. G. Casella and M. Contursi, “Characterization of bismuth adatom-modified palladium electrodes The electrocatalytic oxidation of aliphatic aldehydes in alkaline solutions,” *Electrochim. Acta*, vol. 52, pp. 649–657, 2006.

[45] A. Dutta and J. Datta, “Energy efficient role of Ni/NiO in PdNi nano catalyst used in alkaline DEFC,” *J. Mater. Chem. A*, vol. 2, no. 9, pp. 3237-3250, 2014.

[46] O. Paschos, A. N. Simonov, A. N. Bobrovskaya *et al.*, “Bismuth modified Pd/C as catalysts for hydrogen related reactions,” *Electrochem. commun.*, vol. 12, no. 11, pp. 1490–1492, 2010.

[47] M. M. Tusi, N. S. O. Polanco, S. G. Silva, E. V Spinacé, and A. O. Neto, “Electrochemistry Communications The high activity of PtBi/C electrocatalysts for ethanol electro-oxidation in alkaline medium,” *Electrochem. commun.*, vol. 13, no. 2, pp. 143–146, 2011.

7 List of Figures

8 List of Tables